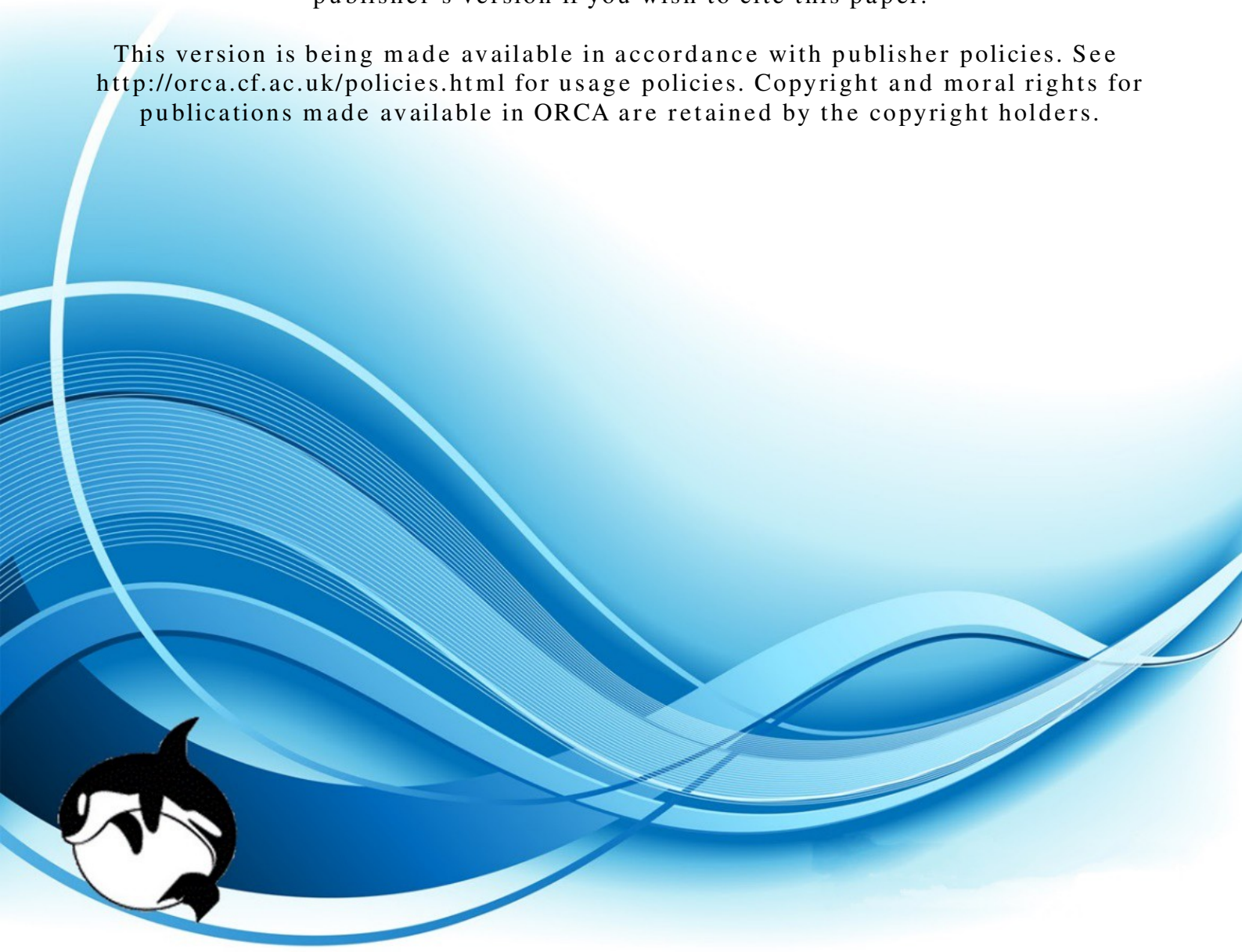

Free vibration of size-dependent FGM Mindlin microplates in viscous fluid

Hui-Cui Li[a], Lin-Feng Zhu[b], Zhangming Wu[c,d], Liao-Liang Ke[a,b]

[a] *Department of Mechanics, Beijing Jiaotong University, Beijing, People's Republic of China*

[b] *School of Mechanical Engineering, Tianjin University, Tianjin, People's Republic of China*

[c] *School of Mechanical Engineering and Mechanics, Ningbo University, Ningbo, People's Republic of China*

[d] *School of Engineering, Cardiff University, Cardiff, United Kingdom of Great Britain and Northern Ireland*

Corresponding author: Liao-Liang Ke; **E-mail:** llke@bjtu.edu.cn

Free vibration of size-dependent functionally graded Mindlin microplates in viscous fluid

Abstract

This paper studies the free vibration of size-dependent functionally graded material (FGM) microplates in contact with viscous fluid. The Mori-Tanaka model is applied to formulate the continuous gradual variation of material properties of FGM microplates along thickness direction. A non-classical microplate model is established based on the modified couple stress theory, which considers the size effect by introducing the material length scale parameter. A physical neutral plane is introduced to eliminate the stretching-bending coupling effect. The motion of viscous fluid is defined by Navier-Stokes equations, with which the hydrodynamic loading on microplates is determined with consideration of inertial effect and viscous damping effect. The governing equations for FGM microplates in contact with viscous fluid are derived using the Hamilton's principle and solved by differential quadrature method. Numerical results are obtained to discuss the influences of the aspect ratio, fluid depth, slenderness ratio, fluid viscosity, gradient index, fluid density, and size parameter on the vibration behaviours of microplates in contact with viscous fluid.

Keywords: FGM microplate; Size effect; Free vibration; Viscous fluid; Fluid-microplate interaction

1. Introduction

Functionally graded materials (FGMs) are inhomogeneous composites that possess gradual variation of material properties by the mixture of two or more materials. The metal and ceramics are the common materials in construction of FGMs, in which their components continuously vary in thickness direction [1]. The performance of FGM structures, especially in extreme environments, can be improved by adjusting the strength and weight distribution. The material property distribution of FGM structures can be described by the power law function [2], linear function [3], exponential function [4], etc. The Voigt model and Mori-Tanaka model are often applied to estimate the effective material properties of FGMs, while Mori-Tanaka model has been widely applicable to a discontinuous particulate phase, especially in microstructures. Kiani and Eslami [5] analyzed the thermal postbuckling behaviour of FGM circular plates and compared the difference of Voigt model, Mori-Tanaka model, and the self-consistent estimate method [6] for the prediction of effective material properties of FGM structures. Shen and Wang [7] studied the difference between the Voigt and Mori-Tanaka models in the application for the nonlinear vibration of FGM plates.

With the rapid progress of fabrication technologies, many microdevices and nanodevices, such as MEMS, NEMS, and biosensors, have been developed and received broad applications in many engineering fields [8, 9]. The investigation on the microscale FGM structures in previous works have observed the size-dependent behaviors from experiments. From the micro-torsion and micro-bending experiments, it was found that the material length scale parameter played a key role on the mechanical behaviors of microscale structures when it was close to the thickness of microscale structures [10]. Therefore, several non-classical continuum theories considering the size effect have been developed, such as the nonlocal theory [11, 12], couple stress theory (CST) [13, 14], strain gradient theory (SGT) [15, 16], and modified couple stress theory (MCST) [17-19]. The modified couple stress theory (MCST) was firstly proposed by Yang et al. [20], which provided an easier way to consider the size effect in the model than the CST, because the MCST included the symmetric tensor and only required one additional scale parameter. Yin et al. [21] presented a vibration study of Kirchhoff microplates based on the MCST, and obtained the natural frequencies of microbeams and microplates.

These non-classical continuum theories in mechanical analysis of FGM microscale structures have been widely employed to analyze the corresponding size effect [22-25]. Based on the MCST, Akbaş [26] contributed the analysis on the vibration of FGM cantilever beams with edge cracks. The bending and vibration behaviors of FGM piezoelectric microplates based on the MCST were studied by Li and Pan [27]. Ke and his collaborators [28, 29] comprehensively discussed the vibration of FGM rectangular and annular microplates with the MCST. By applying the MCST and finite element method, Ma et al. [30] analyzed the vibration of composite Reddy-microplates.

Nowadays, many researchers have increasing research interests to study the vibration of structures in fluid environments because of their potential applications in micro-biosensors, bioprobe, shipbuilding, micro flowmeter, etc [31]. As for homogeneous structures, extensive research efforts have been put forwarded to consider various fluid conditions. When the vibration of structures was coupled with ideal fluid, the hydrodynamic loading was calculated through the potential flow theory [32-34]. In these studies, the inertial effect of the hydrodynamic loading was regarded as the added mass [35] or added virtual mass incremental factors [36]. When the vibration of structures was coupled with compressible fluid, the hydrodynamic loading was calculated through the method of separation of variables [37], Rayleigh's formular [38], contour integration method [39], and finite element method [40].

Except ideal fluid and compressible fluid, the vibration of structures coupled with viscous fluid was also concerned [41-45]. Tuck [46] studied the steady normal oscillation of cylinders in viscous fluid using the Laplace transforms and Green's theorem, and the hydrodynamic loading was approximately computed by removing the singularity with unequal interval quadrature formula. Tuck's method can accurately calculate the hydrodynamic loading for cantilever beams, but it is hard to determine the expression of the hydrodynamic loading for other boundary conditions. Based on the Tuck's method, a detailed theoretical analysis was presented by Sader and his collaborators for the frequency response and hydrodynamic loading of a cantilever beam in viscous fluid [47-49]. Therefore, some approximate methods have been developed to estimate the hydrodynamic loading of other boundary conditions. Golzar et al. [50] analytically investigated the dynamic instability of fluid-loaded microbeams in the cavity of viscous fluid. They used the equivalent squeeze film damping to predict the dynamic response of microbeams with the viscous damping effect. The theory of squeeze film was often used to evaluate the viscosity effect [51]. Wu and Ma [52] applied the double Fourier transform method and Galerkin method to analyze the dynamic characteristics of microplates in contact with compressible viscous fluid. They evaluated the singular integration of the fluid impedance using a quasi-Monte Carlo method. Hosseini-Hashemi et al. [53] focused on the vibration of Kirchhoff nano-plates in contact with viscous fluid based on the nonlocal elastic theory. They derived a simplified expression for the hydrodynamic loading of viscous fluid on nanoplates.

Furthermore, several studies were carried out to analyze the vibration of FGM structures in contact with ideal fluids. Khorshidi et al. [54] conducted the vibration of FGM sandwich microplates in sloshing fluids using the MCST. In bounded ideal fluids, the vibration of FGM microplates considering the effect of surface waves were studied by Bakhsheshy and Mahbadi based on the MCST [55]. Karimi et al. [56] reported the vibration behaviour of FGM microplates in ideal fluids based on the SGT. However, no work had been reported to address the viscosity effect of fluids on the vibration of FGM microbeams and microplates.

In this paper, the size-dependent free vibration of FGM Mindlin microplates in viscous fluid is studied based on the MCST. The Mori-Tanaka method is applied to obtain the local properties of FGM microplates. The in-plane displacements in the Mindlin plate theory are neglected by introducing a physical neutral plane in the model. Both the added mass effect and the viscous damping effect of the hydrodynamic loading on the microplate are considered in the analysis. Hamilton's principle is applied to establish the fluid-microplate coupled equations, which are solved using the differential quadrature (DQ) method. Finally, the influences of the aspect ratio, fluid depth, slenderness ratio, fluid viscosity, gradient index, fluid density, and size parameter on the vibration characteristics of microplates are discussed.

2. Formulation

The schematic of an FGM microplate in contact with viscous fluid is depicted in Figure 1. There is a rectangular tube filled with viscous fluid of height h_f. In this rectangular tube, its bottom part is made of an elastic FGM microplate. As shown in Figure 1(a), only the hydrodynamic loading on its upper surface of the elastic bottom microplate is considered. Figure 1(b) illustrates the spatial geometry of the FGM elastic microplate with thickness h_0, length L_x and width L_y. As shown in Figure 1(b), the coordinate system $Oxyz$ is established for the FGM microplate, in which the microplate is symmetric about the geometric middle plane $z = 0$. For FGM microplates, its components and mechanical properties are normally asymmetric about the geometric middle plane. The physical neutral plane where there are no nonzero components of stresses and strains is introduced to model the FGM microplate, and its location $z = z_0$ varies with respect to the change of the gradient index of FGM microplates.

2.1. Homogenization of material properties

The FGM microplate with components that gradually vary in thickness direction is considered, and its top and bottom surfaces are made of ceramic and metal, respectively. The volume fractions are defined by V_c for ceramic and V_m for metal, and related by $V_m + V_c = 1$. The distribution of ceramic follows a power law function

$$V_c(z) = \left(\frac{1}{2} + \frac{z}{h_0}\right)^n, \tag{1}$$

where subscripts c and m represent the ceramic and metal phases, respectively; n is the gradient index. To capture the local properties of FGM microplates, the Mori-Tanaka method [7] provides an effective way to predict the material properties. The effective Poisson's ratio $\nu(z)$, elastic modulus $E(z)$, and mass density $\rho(z)$ are predicted by the Mori-Tanaka method

$$E(z) = \frac{9K_e(z)\mu_e(z)}{3K_e(z) + \mu_e(z)}, \tag{2}$$

$$\rho(z) = \rho_c V_c(z) + \rho_m V_m(z), \tag{3}$$

$$\nu(z) = \frac{3K_e(z) - 2\mu_e(z)}{6K_e(z) + 2\mu_e(z)}, \tag{4}$$

where

$$\frac{K_e(z) - K_m}{K_c - K_m} = \frac{V_c(z)}{1 + V_m(z)(K_c - K_m)(K_m + 4\mu_m/3)}, \tag{5}$$

$$\frac{\mu_e(z) - \mu_m}{\mu_c - \mu_m} = \frac{V_c(z)}{1 + V_m(z)(\mu_c - \mu_m)/\left[\mu_m + \mu_m(9K_m + 8\mu_m)/6(K_m + 2\mu_m)\right]}, \tag{6}$$

$K_e(z)$ represents the effective value of the bulk modulus and $\mu_e(z)$ denotes the effective value of the shear modulus.

2.2. Hydrodynamic pressure loading

The incompressible viscous fluid is assumed in this fluid-microplate coupling system, and its density and viscosity are ρ_f and μ_f, respectively. The motion of viscous fluid is excited by the vibration of FGM microplates, and the resultant motion of the fluid reacts to the microplates, i.e., this is a fluid-microplate interaction problem. The following Navier-Stokes equation and continuity condition are applied to describe this interaction problem,

$$\rho_f \frac{D\mathbf{v}}{Dt} = -\nabla p + \mu_f \nabla^2 \mathbf{v}, \tag{7}$$

$$\nabla \cdot \mathbf{v} = 0, \tag{8}$$

where p represents the fluid pressure; $\mathbf{v} = (v_x, v_y, v_z)$ is the velocity of viscous fluid. To simplify the problem and derive the analytical solution of the hydrodynamic pressure, the following hypotheses [53] are applied:

(i) The components of velocity and pressure gradient in fluid domain in x- and y- directions are negligible, i.e., $v_x = 0$, $\partial p/\partial x = 0$, $v_y = 0$, and $\partial p/\partial y = 0$.

(ii) The strain component of the microplate in z-direction is zero, i.e., $\partial W/\partial z = 0$.

Based on the first hypotheses, Equation (8) is reduced to $\partial v_z/\partial z = 0$, and Equation (7) is re-written as

$$\rho_f \frac{Dv_z}{Dt} = -\frac{\partial p}{\partial z} + \mu_f \left(\frac{\partial^2 v_z}{\partial x^2} + \frac{\partial^2 v_z}{\partial y^2} \right). \tag{9}$$

The interfacial conditions between the viscous fluid and microplate are

$$\begin{aligned} v_z &= \frac{DW}{Dt} = \frac{\partial W}{\partial t} + v_x \frac{\partial W}{\partial x} + v_y \frac{\partial W}{\partial y} + v_z \frac{\partial W}{\partial z} = \frac{\partial W}{\partial t}, \\ \dot{v}_z &= \frac{Dv_z}{Dt} = \frac{\partial v_z}{\partial t} + v_x \frac{\partial v_z}{\partial x} + v_y \frac{\partial v_z}{\partial y} + v_z \frac{\partial v_z}{\partial z} = \frac{\partial^2 W}{\partial t^2}, \end{aligned} \tag{10}$$

where v_z and W are the z-axial fluid velocity and microplate displacement, respectively; the operator D/Dt refers to the material derivative about time t. Substituting Equation (10) into

Equation (9), the pressure gradient at the interface between the fluid and microplate is

$$\left.\frac{\partial p}{\partial z}\right|_{z=\frac{h_0}{2}} = -\rho_f \frac{\partial^2 W}{\partial t^2} + \mu_f \left(\frac{\partial^3 W}{\partial x^2 \partial t} + \frac{\partial^3 W}{\partial y^2 \partial t} \right). \tag{11}$$

Regardless of the gravity effect of fluid, the hydrodynamic loading on the fluid-microplate interface is given by

$$F_{fluid} = h_f \frac{\partial p}{\partial z} = -h_f \rho_f \frac{\partial^2 W}{\partial t^2} + h_f \mu_f \left(\frac{\partial^3 W}{\partial x^2 \partial t} + \frac{\partial^3 W}{\partial y^2 \partial t} \right), \tag{12}$$

where the first and second terms on the right-hand side of Equation (12) correspond to the added mass effect and viscosity damping effect, respectively.

2.3. The modified couple stress theory

In the analysis of microplates, the size dependent effect can be predicted by using the modified couple stress theory (MCST). Based on MCST described by Yang et al. [20], the strain energy Π_S of microplates is given by

$$\Pi_s = \frac{1}{2}\int_{\Lambda} (\boldsymbol{\sigma} : \boldsymbol{\varepsilon} + \mathbf{m} : \boldsymbol{\chi}) \mathrm{d}\Lambda, \tag{13}$$

where Λ denotes the domain occupied by FGM microplates; tensor $\boldsymbol{\sigma}$ and $\mathbf{m}$ denote the Cauchy stress and deviatoric part of the couple stress, respectively; tensor $\boldsymbol{\varepsilon}$ and $\boldsymbol{\chi}$ denote the Cauchy strain and symmetric curvature, respectively. They are formulated as

$$\boldsymbol{\sigma} = \lambda \mathrm{tr}(\boldsymbol{\varepsilon})\mathbf{I} + 2\mu\boldsymbol{\varepsilon}, \tag{14}$$

$$\boldsymbol{\varepsilon} = \frac{1}{2}\left[\nabla \mathbf{u} + (\nabla \mathbf{u})^{\mathrm{T}} \right], \tag{15}$$

$$\mathbf{m} = 2l^2 \mu \boldsymbol{\chi}, \tag{16}$$

$$\boldsymbol{\chi} = \frac{1}{2}\left[\nabla \boldsymbol{\theta} + (\nabla \boldsymbol{\theta})^{\mathrm{T}} \right], \tag{17}$$

where l represents the scale parameter; the displacement vector $\mathbf{u} = \left(\tilde{U}, \tilde{V}, \tilde{W}\right)$ is expressed in Equation (19); μ and λ denote Lame's constants; the rotation vector $\boldsymbol{\theta}$ is

$$\boldsymbol{\theta} = \frac{1}{2}\mathrm{curl}\ \mathbf{u}.$$

2.4. Vibration of FGM microplates

The components and physical properties of the FGM microplate are often asymmetric about the geometric mid-plane. By introducing the physical neutral plane in the model of FGM microplates, it results in no stretching-bending coupling effect in the vibration analysis of FGM microplates. The location of the neutral plane $z = z_0$ is determined by the following expression [57]:

$$z_0 = \int_{-h_0/2}^{h_0/2} \frac{E(z)z}{1-\nu^2(z)}\mathrm{d}z \Big/ \int_{-h_0/2}^{h_0/2} \frac{E(z)}{1-\nu^2(z)}\mathrm{d}z\,. \tag{18}$$

Specifically, the neutral plane is coincided with the geometric mid-plane for homogeneous plates. The effect of in-plane displacements can be neglected through the introduction of the neutral plane due to their independence of the out-of-plane deflection. Based on the Mindlin plate theory, the displacements **u** of FGM microplates are given by [29,58]

$$\mathbf{u} = \begin{pmatrix} \tilde{U}(x,y,z,t) \\ \tilde{V}(x,y,z,t) \\ \tilde{W}(x,y,z,t) \end{pmatrix} = \begin{pmatrix} (z-z_0)\Psi_x(x,y,t) \\ (z-z_0)\Psi_y(x,y,t) \\ W(x,y,t) \end{pmatrix}, \tag{19}$$

where W represents the out-of-plane deflection of the physical neutral plane; $\tilde{U}$, $\tilde{V}$, and $\tilde{W}$ denote the x-, y-, and z-axial displacement components, respectively; Ψ_x and Ψ_y refer to the rotations of the physical neutral plane about y- and x-axes, respectively. Note that the Kirchhoff plate theory can be obtained by setting $\Psi_x = -\mathrm{d}W/\mathrm{d}x$ and $\Psi_y = -\mathrm{d}W/\mathrm{d}y$. The stress tensor **σ** in Equation (14) are

$$\sigma_{xx} = Q_{11}\varepsilon_{xx} + Q_{12}\varepsilon_{yy},\ \sigma_{yy} = Q_{11}\varepsilon_{yy} + Q_{12}\varepsilon_{xx},\ \sigma_{xy} = Q_{66}\varepsilon_{xy},\ \sigma_{yz} = Q_{66}\varepsilon_{yz},\ \sigma_{xz} = Q_{66}\varepsilon_{xz}, \tag{20}$$

where **ε** is strain tensor, its nonzero components are expressed as

$$\begin{aligned} &\varepsilon_{xx} = (z-z_0)\frac{\partial\Psi_x}{\partial x}, \varepsilon_{xy} = (z-z_0)\left(\frac{\partial\Psi_x}{\partial y} + \frac{\partial\Psi_y}{\partial x}\right),\ \varepsilon_{yy} = (z-z_0)\frac{\partial\Psi_y}{\partial y}, \\ &\varepsilon_{xz} = \Psi_x + \frac{\partial W}{\partial x},\ \varepsilon_{yz} = \Psi_y + \frac{\partial W}{\partial y}, \end{aligned} \tag{21}$$

and stiffness components are

$$Q_{11} = \frac{E(z)}{1-\nu^2(z)},\ Q_{66} = \frac{E(z)}{2[1+\nu(z)]},\ Q_{12} = \frac{\nu(z)E(z)}{1-\nu^2(z)}. \tag{22}$$

According to Equation (17), curvature tensor **χ** is

$$\begin{aligned} &\chi_{xx} = \frac{1}{2}\left(\frac{\partial^2 W}{\partial x\partial y} - \frac{\partial\Psi_y}{\partial x}\right),\ \chi_{yy} = \frac{1}{2}\left(\frac{\partial\Psi_x}{\partial y} - \frac{\partial^2 W}{\partial x\partial y}\right), \\ &\chi_{zz} = \frac{1}{2}\left(\frac{\partial\Psi_y}{\partial x} - \frac{\partial\Psi_x}{\partial y}\right),\ \chi_{xy} = \frac{1}{4}\left(\frac{\partial^2 W}{\partial y^2} - \frac{\partial^2 W}{\partial x^2} + \frac{\partial\Psi_x}{\partial x} - \frac{\partial\Psi_y}{\partial y}\right), \\ &\chi_{xz} = \frac{(z-z_0)}{4}\left(\frac{\partial^2\Psi_y}{\partial x^2} - \frac{\partial^2\Psi_x}{\partial x\partial y}\right),\ \chi_{yz} = \frac{(z-z_0)}{4}\left(\frac{\partial^2\Psi_y}{\partial x\partial y} - \frac{\partial^2\Psi_x}{\partial x^2}\right), \end{aligned} \tag{23}$$

and the rotation vector θ is

$$\theta_x = -\frac{1}{2}\left(\Psi_y - \frac{\partial W}{\partial y}\right),\ \theta_y = \frac{1}{2}\left(\Psi_x - \frac{\partial W}{\partial x}\right),\ \theta_z = \frac{(z-z_0)}{2}\left(\frac{\partial\Psi_y}{\partial x} - \frac{\partial\Psi_x}{\partial y}\right). \tag{24}$$

The couple moments $\{Y_{xx}, Y_{xy}, Y_{yy}, Y_{zz}\}$, bending moments $\{M_{xx}, M_{xy}, M_{yy}\}$, transverse shear forces $\{Q_x, Q_y\}$, and high-order couple moments $\{T_{xy}, T_{yz}\}$ are [29]

$$\begin{Bmatrix} M_{xx} \\ M_{yy} \\ M_{xy} \end{Bmatrix} = \int_{-h_0/2}^{h_0/2} \begin{Bmatrix} \sigma_{xx} \\ \sigma_{yy} \\ \sigma_{xy} \end{Bmatrix} (z - z_0)\,\mathrm{d}z = \begin{Bmatrix} D_{11}\,\partial\Psi_x/\partial x + D_{12}\,\partial\Psi_y/\partial y \\ D_{11}\,\partial\Psi_y/\partial y + D_{12}\,\partial\Psi_x/\partial x \\ D_{66}\left(\partial\Psi_x/\partial y + \partial\Psi_y/\partial x\right) \end{Bmatrix}, \tag{25a}$$

$$\begin{Bmatrix} Q_x \\ Q_y \end{Bmatrix} = \kappa \int_{-h_0/2}^{h_0/2} \begin{Bmatrix} \sigma_{xz} \\ \sigma_{yz} \end{Bmatrix} \mathrm{d}z = \kappa A_{66} \begin{Bmatrix} \Psi_x + \partial W/\partial x \\ \Psi_y + \partial W/\partial y \end{Bmatrix}, \tag{25b}$$

$$\begin{Bmatrix} Y_{xx} \\ Y_{yy} \\ Y_{zz} \\ Y_{xy} \end{Bmatrix} = \int_{-h_0/2}^{h_0/2} \begin{Bmatrix} m_{xx} \\ m_{yy} \\ m_{zz} \\ m_{xy} \end{Bmatrix} \mathrm{d}z = 2A_{66}l^2 \begin{Bmatrix} \left(\partial^2 W/\partial x\partial y + \partial\Psi_y/\partial x\right)/2 \\ \left(\partial\Psi_x/\partial y - \partial^2 W/\partial x\partial y\right)/2 \\ \left(\partial\Psi_y/\partial x - \partial\Psi_x/\partial y\right)/2 \\ \left(\partial^2 W/\partial y^2 - \partial^2 W/\partial x^2 + \partial\Psi_x/\partial x - \partial\Psi_y/\partial y\right)/4 \end{Bmatrix}, \tag{25c}$$

$$\begin{Bmatrix} T_{xz} \\ T_{yz} \end{Bmatrix} = \int_{-h_0/2}^{h_0/2} \begin{Bmatrix} m_{xz} \\ m_{yz} \end{Bmatrix} (z - z_0)\,\mathrm{d}z = 2D_{66}l^2 \begin{Bmatrix} \left(\partial^2\Psi_y/\partial x^2 - \partial^2\Psi_x/\partial x\partial y\right)/4 \\ \left(\partial^2\Psi_y/\partial x\partial y - \partial^2\Psi_x/\partial y^2\right)/4 \end{Bmatrix}, \tag{25d}$$

where $\kappa = 5/6$ is taken to approximate the shear correction factor. The terms of stiffness and inertia are defined as

$$A_{66} = \int_{-h_0/2}^{h_0/2} Q_{66}\mathrm{d}z,\ \{D_{11}, D_{12}, D_{66}\} = \int_{-h_0/2}^{h_0/2} \{Q_{11}, Q_{12}, Q_{66}\}(z - z_0)^2\,\mathrm{d}z,$$
$$\{I_1, I_3\} = \int_{-h_0/2}^{h_0/2} \rho(z)\left\{1, (z - z_0)^2\right\}\mathrm{d}z.$$

According to the Hamilton principle

$$\int_0^t (\delta\Pi_S - \delta\Pi_T + \delta\Pi_F)\mathrm{d}t = 0, \tag{26}$$

where the strain energy Π_S includes two parts, i.e., $\Pi_S = \Pi_{SC} + \Pi_{SNC}$. Π_{SC} is the strain energy derived from the classical thin plate theory, and Π_{SNC} denotes the strain energy contributed by introducing the MCST. They are formulated as:

$$\begin{aligned} \Pi_{SC} &= \frac{1}{2}\int_0^{L_y}\int_0^{L_x} \sigma_{ij}\varepsilon_{ij}\mathrm{d}x\mathrm{d}y = \frac{1}{2}\int_0^{L_y}\int_0^{L_x} \left[M_{xx}\frac{\partial\Psi_x}{\partial x} + M_{yy}\frac{\partial\Psi_y}{\partial y} \right. \\ &\left. + Q_x\left(\Psi_x + \frac{\partial W}{\partial x}\right) + M_{xy}\left(\frac{\partial\Psi_x}{\partial y} + \frac{\partial\Psi_y}{\partial x}\right) + Q_y\left(\Psi_y + \frac{\partial W}{\partial y}\right)\right]\mathrm{d}x\mathrm{d}y, \end{aligned} \tag{27}$$

$$\begin{aligned} \Pi_{SNC} &= \frac{1}{2}\int_0^{L_y}\int_0^{L_x} m_{ij}\chi_{ij}\mathrm{d}x\mathrm{d}y = \frac{1}{2}\int_0^{L_y}\int_0^{L_x} \left[\frac{Y_{xx}}{2}\left(\frac{\partial^2 W}{\partial x\partial y} - \frac{\partial\Psi_y}{\partial x}\right) \right. \\ &+ \frac{Y_{yy}}{2}\left(\frac{\partial\Psi_x}{\partial y} - \frac{\partial^2 W}{\partial x\partial y}\right) + \frac{Y_{xy}}{2}\left(\frac{\partial^2 W}{\partial y^2} - \frac{\partial^2 W}{\partial x^2} + \frac{\partial\Psi_x}{\partial x} - \frac{\partial\Psi_y}{\partial y}\right) \\ &\left. + \frac{Y_{zz}}{2}\left(\frac{\partial\Psi_y}{\partial x} - \frac{\partial\Psi_x}{\partial y}\right) + \frac{T_{xz}}{2}\left(\frac{\partial^2\Psi_y}{\partial x^2} - \frac{\partial^2\Psi_x}{\partial x\partial y}\right) + \frac{T_{yz}}{2}\left(\frac{\partial^2\Psi_y}{\partial x\partial y} - \frac{\partial^2\Psi_x}{\partial x^2}\right)\right]\mathrm{d}x\mathrm{d}y. \end{aligned} \tag{28}$$

The kinetic energy Π_T is:

$$\Pi_T = \frac{1}{2}\int_0^{L_y}\int_0^{L_x}\left\{I_1\left(\frac{\partial W}{\partial t}\right)^2 + I_3\left[\left(\frac{\partial \Psi_x}{\partial t}\right)^2 + \left(\frac{\partial \Psi_y}{\partial t}\right)^2\right]\right\}\mathrm{d}x\mathrm{d}y\,. \tag{29}$$

The external work of microplates Π_F due to the hydrodynamic loading of viscous fluid at the fluid-microplate interface is:

$$\Pi_F = \frac{1}{2}\int_0^{L_y}\int_0^{L_x} F_{fluid}(x,y,t)W\mathrm{d}x\mathrm{d}y\,, \tag{30}$$

where the hydrodynamic loading is expressed by Equation (12).

Using the integration by parts, the governing equations of the microplate-fluid system are obtained

$$\begin{aligned}&\frac{\partial Q_x}{\partial x} - \frac{1}{2}\left(\frac{\partial^2 Y_{xx}}{\partial x\partial y} - \frac{\partial^2 Y_{yy}}{\partial x\partial y} + \frac{\partial^2 Y_{xy}}{\partial y^2} - \frac{\partial^2 Y_{xy}}{\partial x^2}\right) + \frac{\partial Q_y}{\partial y}\\ &= -h_f\mu_f\left(\frac{\partial^3 W}{\partial x^2\partial t} + \frac{\partial^3 W}{\partial y^2\partial t}\right) + \left(I_1 + h_f\rho_f\right)\frac{\partial^2 W}{\partial t^2},\end{aligned} \tag{31}$$

$$\frac{\partial M_{xx}}{\partial x} + \frac{\partial M_{xy}}{\partial y} - Q_x - \frac{1}{2}\left(\frac{\partial Y_{zz}}{\partial y} - \frac{\partial Y_{yy}}{\partial y} - \frac{\partial Y_{xy}}{\partial x} - \frac{\partial^2 T_{xz}}{\partial x\partial y} - \frac{\partial^2 T_{yz}}{\partial y^2}\right) = I_3\frac{\partial^2 \Psi_x}{\partial t^2}\,, \tag{32}$$

$$\frac{\partial M_{xy}}{\partial x} + \frac{\partial M_{yy}}{\partial y} - Q_y - \frac{1}{2}\left(\frac{\partial Y_{xx}}{\partial x} - \frac{\partial Y_{zz}}{\partial x} + \frac{\partial Y_{xy}}{\partial y} + \frac{\partial^2 T_{xz}}{\partial x^2} + \frac{\partial^2 T_{yz}}{\partial x\partial y}\right) = I_3\frac{\partial^2 \Psi_y}{\partial t^2}\,, \tag{33}$$

and the relevant boundary conditions require

$$\begin{aligned}&W = 0 \text{ or } \left(Q_x - \frac{1}{4}\frac{\partial Y_{xx}}{\partial y} + \frac{1}{4}\frac{\partial Y_{yy}}{\partial y} + \frac{1}{2}\frac{\partial Y_{xy}}{\partial x}\right)n_x + \left(Q_y - \frac{1}{4}\frac{\partial Y_{xx}}{\partial x} + \frac{1}{4}\frac{\partial Y_{yy}}{\partial x} + \frac{1}{2}\frac{\partial Y_{xy}}{\partial y}\right)n_y = 0,\\ &\frac{\partial W}{\partial x} = 0 \text{ or } \frac{1}{2}Y_{xy}n_x + \left(\frac{1}{4}Y_{xx} - \frac{1}{4}Y_{yy}\right)n_y = 0,\quad \frac{\partial W}{\partial y} = 0 \text{ or } \left(\frac{1}{4}Y_{xx} - \frac{1}{4}Y_{yy}\right)n_x + \frac{1}{2}Y_{xy}n_y = 0,\end{aligned} \tag{34a}$$

$$\begin{aligned}&\Psi_x = 0 \text{ or } \left(M_{xx} + \frac{1}{2}Y_{xy} + \frac{1}{4}\frac{\partial T_{xz}}{\partial y}\right)n_x + \left(M_{xy} + \frac{1}{2}Y_{yy} - \frac{1}{2}Y_{zz} + \frac{1}{2}\frac{\partial T_{yz}}{\partial y} + \frac{1}{4}\frac{\partial T_{xz}}{\partial x}\right)n_y = 0,\\ &\frac{\partial \Psi_x}{\partial x} = 0 \text{ or } \frac{1}{4}T_{yz}n_y = 0,\quad \frac{\partial \Psi_x}{\partial y} = 0 \text{ or } -\frac{1}{4}T_{xz}n_x - \frac{1}{2}T_{yz}n_y = 0,\end{aligned} \tag{34b}$$

$$\begin{aligned}&\Psi_y = 0 \text{ or } \left(M_{xy} + \frac{1}{2}Y_{xx} + \frac{1}{2}Y_{zz} + \frac{1}{4}\frac{\partial T_{yz}}{\partial y} + \frac{1}{2}\frac{\partial T_{xz}}{\partial x}\right)n_x + \left(M_{yy} - \frac{1}{2}Y_{xy} - \frac{1}{4}\frac{\partial T_{yz}}{\partial x}\right)n_y = 0,\\ &\frac{\partial \Psi_y}{\partial x} = 0 \text{ or } \frac{1}{2}T_{xz}n_x + \frac{1}{4}T_{yz}n_y = 0,\quad \frac{\partial \Psi_y}{\partial y} = 0 \text{ or } \frac{1}{4}T_{yz}n_x = 0,\end{aligned} \tag{34c}$$

where n_x and n_y are the direction cosines of unit normal vectors normal to the physical neutral plane. Several parameters are normalized as

$$w = \frac{W}{h_0},\ \zeta = \frac{x}{L_x},\ \xi = \frac{y}{L_y},\ (\eta_1,\eta_2) = \frac{(L_x,L_y)}{h_0},\ l_0 = \frac{l}{h_0},\ (\psi_x,\psi_y) = (\Psi_x,\Psi_y)\,, \tag{35a}$$

$$a_{66}=\frac{A_{66}}{A_{110}},\ \left(d_{11},d_{12},d_{66}\right)=\frac{\left(D_{11},D_{12},D_{66}\right)}{A_{110}h_0^2},\ \left(\overline{I}_1,\overline{I}_3,\overline{I}_f\right)=\left(\frac{I_1}{I_{10}},\frac{I_3}{I_{10}h_0^2},\frac{h_f\rho_f}{I_{10}}\right), \tag{35b}$$

$$\lambda=\frac{L_x}{L_y},\ \overline{h}_f=\frac{h_f}{I_{10}/\rho_f},\ \Omega_0=\frac{1}{L_x}\sqrt{\frac{A_{110}}{I_{10}}},\overline{\mu}_f=\frac{\mu_f}{\rho_f\Omega L_x^2},\ \tau=\Omega_0 t,\omega=\frac{\Omega}{\Omega_0}, \tag{35c}$$

where l_0 is the non-dimensional size parameter; η_1 and η_2 are the length-thickness ratio and width-thickness ratio of microplates, respectively; I_{10} and A_{110} are equal to I_1 and A_{11} of homogeneous plates, respectively; λ defines the aspect ratio; $\overline{\mu}_f$ represents the fluid viscosity and $\overline{h}_f$ is the dimensionless fluid depth; Ω is the complex parameter and ω is its normalized form.

The dimensionless forms of Equations (31)-(33) are

$$\begin{aligned}&\kappa a_{66}\left(\frac{\partial^2 w}{\partial\zeta^2}+\eta_1\frac{\partial\psi_x}{\partial\zeta}+\lambda^2\frac{\partial^2 w}{\partial\xi^2}+\lambda\eta_1\frac{\partial\psi_y}{\partial\xi}\right)-\frac{l_0^2}{4}a_{66}\left(\frac{1}{\eta_1^2}\frac{\partial^4 w}{\partial\zeta^4}+\frac{\lambda^2}{\eta_2^2}\frac{\partial^4 w}{\partial\xi^4}\right.\\&\left.+\frac{2}{\eta_2^2}\frac{\partial^4 w}{\partial\zeta^2\partial\xi^2}-\frac{1}{\eta_1}\frac{\partial^3\psi_x}{\partial\zeta^3}-\frac{\lambda^2}{\eta_2}\frac{\partial^3\psi_y}{\partial\xi^3}-\frac{\lambda}{\eta_2}\frac{\partial^3\psi_x}{\partial\zeta\partial\xi^2}-\frac{1}{\eta_2}\frac{\partial^3\psi_y}{\partial\zeta^2\partial\xi}\right)\\&+\overline{I}_f\overline{\mu}_f\frac{\partial}{\partial\tau}\left(\frac{\partial^2 w}{\partial\zeta^2}+\lambda^2\frac{\partial^2 w}{\partial\xi^2}\right)=\left(\overline{I}_1+\overline{I}_f\right)\frac{\partial^2 w_i}{\partial\tau^2},\end{aligned} \tag{36}$$

$$\begin{aligned}&d_{11}\frac{\partial^2\psi_x}{\partial\zeta^2}+\lambda(d_{12}+d_{66})\frac{\partial^2\psi_y}{\partial\zeta\partial\xi}+\lambda^2 d_{66}\frac{\partial^2\psi_x}{\partial\xi^2}-\kappa a_{66}\left(\eta_1\frac{\partial w}{\partial\zeta}+\eta_1^2\psi_x\right)\\&-\frac{l_0^2}{4}a_{66}\left(\frac{\lambda}{\eta_2}\frac{\partial^3 w}{\partial\zeta\partial\xi^2}+\frac{1}{\eta_1}\frac{\partial^3 w}{\partial\zeta^3}+3\lambda\frac{\partial^2\psi_y}{\partial\zeta\partial\xi}-4\lambda^2\frac{\partial^3\psi_x}{\partial\xi^3}-\frac{\partial^2\psi_x}{\partial\zeta^2}\right)+\\&\frac{l_0^2}{4}d_{66}\left(\frac{1}{\eta_1\eta_2}\frac{\partial^4\psi_y}{\partial\zeta^3\partial\xi}-\frac{1}{\eta_2^2}\frac{\partial^4\psi_x}{\partial\zeta^2\partial\xi^2}-\frac{\lambda^2}{\eta_2^2}\frac{\partial^4\psi_x}{\partial\xi^4}+\frac{\lambda}{\eta_2^2}\frac{\partial^4\psi_y}{\partial\zeta\partial\xi^3}\right)=\overline{I}_3\frac{\partial^2\psi_x}{\partial\tau^2},\end{aligned} \tag{37}$$

$$\begin{aligned}&d_{11}\frac{\partial^2\psi_y}{\partial\xi^2}+\lambda(d_{12}+d_{66})\frac{\partial^2\psi_x}{\partial\zeta\partial\xi}+d_{66}\frac{\partial^2\psi_y}{\partial\zeta^2}-\kappa a_{66}\left(\lambda\eta_1\frac{\partial w}{\partial\xi}+\eta_1^2\psi_y\right)\\&-\frac{l_0^2}{4}a_{66}\left(\frac{1}{\eta_2}\frac{\partial^3 w}{\partial\zeta^2\partial\xi}+\frac{\lambda^2}{\eta_2}\frac{\partial^3 w}{\partial\xi^3}-4\frac{\partial^3\psi_y}{\partial\zeta^3}+3\lambda\frac{\partial^2\psi_x}{\partial\zeta\partial\xi}-\lambda^2\frac{\partial^2\psi_y}{\partial\xi^2}\right)+\\&\frac{l_0^2}{4}d_{66}\left(\frac{1}{\eta_1\eta_2}\frac{\partial^4\psi_x}{\partial\zeta^3\partial\xi}+\frac{\lambda}{\eta_2^2}\frac{\partial^4\psi_x}{\partial\zeta\partial\xi^3}-\frac{1}{\eta_2^2}\frac{\partial^4\psi_y}{\partial\zeta^2\partial\xi^2}-\frac{1}{\eta_2^2}\frac{\partial^4\psi_y}{\partial\zeta^4}\right)=\overline{I}_3\frac{\partial^2\psi_y}{\partial\tau^2},\end{aligned} \tag{38}$$

The non-dimensional boundary conditions are:

$$w=\frac{\partial w}{\partial\zeta}=\psi_x=\frac{\partial\psi_x}{\partial\zeta}=\psi_y=\frac{\partial\psi_y}{\partial\zeta}=0,\ \text{at}\ \ \zeta=0\ \text{and}\ \ \zeta=1, \tag{39a}$$

$$w=\frac{\partial w}{\partial\xi}=\psi_x=\frac{\partial\psi_x}{\partial\xi}=\psi_y=\frac{\partial\psi_y}{\partial\xi}=0,\ \text{at}\ \ \xi=0\ \text{and}\ \ \xi=1, \tag{39b}$$

for all edges clamped (CCCC) microplates. The non-dimensional forms of boundary conditions are

$$w=\psi_y=0,\ M_{xx}=d_{11}\frac{\partial\psi_x}{\partial\zeta}+\lambda d_{12}\frac{\partial\psi_y}{\partial\xi}=0,\ Y_{xy}=\lambda^2\frac{\partial^2 w}{\partial\xi^2}-\frac{\partial^2 w}{\partial\zeta^2}+\eta_1\frac{\partial\psi_x}{\partial\zeta}-\lambda\eta_1\frac{\partial\psi_y}{\partial\xi}=0,$$
$$T_{xz}=\frac{\partial^2\psi_y}{\partial\zeta^2}-\lambda\frac{\partial^2\psi_x}{\partial\zeta\partial\xi}=0,\ T_{yz}=\frac{\partial^2\psi_y}{\partial\zeta\partial\xi}-\lambda\frac{\partial^2\psi_x}{\partial\xi^2}=0,\ \text{at}\ \ \zeta=0\ \text{and}\ \ \zeta=1, \tag{40a}$$

$$w=\psi_x=0,\ M_{yy}=d_{11}\lambda\frac{\partial\psi_y}{\partial\xi}+d_{12}\frac{\partial\psi_x}{\partial\zeta}=0,\ Y_{xy}=\lambda^2\frac{\partial^2 w}{\partial\xi^2}-\frac{\partial^2 w}{\partial\zeta^2}+\eta_1\frac{\partial\psi_x}{\partial\zeta}-\lambda\eta_1\frac{\partial\psi_y}{\partial\xi}=0,$$
$$T_{xz}=\frac{\partial^2\psi_y}{\partial\zeta^2}-\lambda\frac{\partial^2\psi_x}{\partial\zeta\partial\xi}=0,\ T_{yz}=\frac{\partial^2\psi_y}{\partial\zeta\partial\xi}-\lambda\frac{\partial^2\psi_x}{\partial\xi^2}=0,\ \text{at}\ \ \xi=0\ \text{and}\ \ \xi=1, \tag{40b}$$

for all edges simply supported (SSSS) microplates.

2.5. Solution method

In this work, the DQ method is a numerical technique to solve Equations (36)-(40) through the discretization of unknown variables w, ψ_x, ψ_y and their p_1th, p_2th partial derivatives as,

$$\left\{w,\psi_x,\psi_y\right\}=\sum_{n=1}^{N}\sum_{m=1}^{M}l_n(\zeta)l_m(\xi)\left\{w_{mn},\psi_{xmn},\psi_{ymn}\right\}, \tag{41}$$

$$\frac{\partial^{p_1}}{\partial\xi^{p_1}}\frac{\partial^{p_2}}{\partial\zeta^{p_2}}\left\{w,\psi_x,\psi_y\right\}\Big|_{\zeta=\zeta_{k_1},\xi=\xi_{k_2}}=\sum_{n=1}^{N}\sum_{m=1}^{M}C_{k_2m}^{p_1}(\xi)C_{k_1n}^{p_2}(\zeta)\left\{w_{mn},\psi_{xmn},\psi_{ymn}\right\}, \tag{42}$$

where $N\times M$ are the total number of sampling points. The selection of sampling points obeys the Chebyshev-Gauss-Lobatto collocation method [59] as

$$\zeta_{k_1}=\frac{1}{2}\left\{1-\cos\left[\frac{\pi(k_1-1)}{N-1}\right]\right\},\ k_1=1,2,\ldots N, \tag{43}$$

$$\xi_{k_2}=\frac{1}{2}\left\{1-\cos\left[\frac{\pi(k_2-1)}{M-1}\right]\right\},\ k_2=1,2,\ldots M, \tag{44}$$

where ζ_{k_1} and ξ_{k_2} are the values of k_1th and k_2th sampling points along the ζ- and ξ- directions, respectively; the subscripts n and m correspond to the values at ζ_n and ξ_m, respectively; Lagrange interpolation polynomials $l_m(\xi)$, $l_n(\zeta)$, and weighted coefficients $C_{k_2m}^{p_1}(\xi)$, $C_{k_1n}^{p_2}(\zeta)$ are given in Shu [59].

Then, Equations (36)-(40) are discretized as

$$\begin{aligned}
&\kappa a_{66}\left[\sum_{n=1}^{N}C_{k_1n}^{(2)}w_{nk_2}+\eta_i\sum_{n=1}^{N}C_{k_1n}^{(1)}\psi_{xnk_2}+\eta_1\lambda\sum_{m=1}^{M}C_{k_2m}^{(1)}\psi_{yk_1m}+\lambda^2\sum_{m=1}^{M}C_{k_2m}^{(2)}w_{k_1m}\right]-\frac{l_0^2}{4}a_{66}\\
&\left[\frac{1}{\eta_1^2}\sum_{n=1}^{N}C_{k_1n}^{(4)}w_{nk_2}+\frac{\lambda^2}{\eta_2^2}\sum_{m=1}^{M}C_{k_2m}^{(4)}w_{k_1m}+\frac{2}{\eta_2^2}\sum_{n=1}^{N}\sum_{m=1}^{M}C_{k_1n}^{(2)}C_{k_2m}^{(2)}w_{nm}-\frac{1}{\eta_1}\sum_{n=1}^{N}C_{k_1n}^{(3)}\psi_{xnk_2}\right.\\
&\left.-\frac{\lambda^2}{\eta_2}\sum_{m=1}^{M}C_{k_2m}^{(3)}\psi_{yk_1m}-\frac{\lambda}{\eta_2}\sum_{n=1}^{N}\sum_{m=1}^{M}C_{k_1n}^{(1)}C_{k_2m}^{(2)}\psi_{xnm}-\frac{1}{\eta_2}\sum_{n=1}^{N}\sum_{m=1}^{M}C_{k_1n}^{(2)}C_{k_2m}^{(1)}\psi_{ynm}\right]\\
&+\bar{I}_f\bar{\mu}_f\left[\sum_{n=1}^{N}C_{k_1n}^{(2)}\dot{w}_{nk_2}+\lambda^2\sum_{m=1}^{M}C_{k_2m}^{(2)}\dot{w}_{k_1m}\right]=\left(\bar{I}_1+\bar{I}_f\right)\ddot{w}_{ik_1k_2},
\end{aligned} \tag{45}$$

$$
\begin{aligned}
&d_{11}\sum_{n=1}^{N}C_{k_1n}^{(2)}\psi_{xnk_2}+\lambda(d_{12}+d_{66})\sum_{n=1}^{N}\sum_{m=1}^{M}C_{k_1n}^{(1)}C_{k_2m}^{(1)}\psi_{ynm}-\kappa a_{66}\left[\eta_1\sum_{n=1}^{N}C_{k_1n}^{(1)}w_{nk_2}+\eta_1{}^2\psi_{xk_1k_2}\right]\\
&+\lambda^2 d_{66}\sum_{m=1}^{M}C_{k_2m}^{(2)}\psi_{xk_1m}-\frac{l_0^2}{4}a_{66}\left[\frac{\lambda}{\eta_2}\sum_{n=1}^{N}\sum_{m=1}^{M}C_{k_1n}^{(1)}C_{k_2m}^{(2)}w_{nm}+\frac{1}{\eta_1}\sum_{n=1}^{N}C_{k_1n}^{(3)}w_{nk_2}-4\lambda^2\sum_{m=1}^{M}C_{k_2m}^{(3)}\psi_{xk_1m}\right.\\
&\left.+3\lambda\sum_{n=1}^{N}\sum_{m=1}^{M}C_{k_1n}^{(1)}C_{k_2m}^{(1)}\psi_{ynm}-\sum_{n=1}^{N}C_{k_1n}^{(2)}\psi_{xnk_2}\right]+\frac{l_0^2}{4}d_{66}\left[\frac{1}{\eta_1\eta_2}\sum_{n=1}^{N}\sum_{m=1}^{M}C_{k_1n}^{(3)}C_{k_2m}^{(1)}\psi_{ynm}\right.\\
&\left.+\frac{\lambda}{\eta_2^2}\sum_{n=1}^{N}\sum_{m=1}^{M}C_{k_1n}^{(1)}C_{k_2m}^{(3)}\psi_{ynm}-\frac{1}{\eta_2^2}\sum_{n=1}^{N}\sum_{m=1}^{M}C_{k_1n}^{(2)}C_{k_2m}^{(2)}\psi_{xnm}-\frac{\lambda^2}{\eta_2^2}\sum_{m=1}^{M}C_{k_2m}^{(4)}\psi_{xk_1m}\right]=\bar{I}_3\ddot{\psi}_{xk_1k_2},
\end{aligned}
\tag{46}
$$

$$
\begin{aligned}
&d_{11}\sum_{n=1}^{N}C_{k_1n}^{(2)}\psi_{xnk_2}+\lambda(d_{12}+d_{66})\sum_{n=1}^{N}\sum_{m=1}^{M}C_{k_1n}^{(1)}C_{k_2m}^{(1)}\psi_{ynm}-\kappa a_{66}\left[\eta_1\sum_{n=1}^{N}C_{k_1n}^{(1)}w_{nk_2}+\eta_1{}^2\psi_{xk_1k_2}\right]\\
&+\lambda^2 d_{66}\sum_{m=1}^{M}C_{k_2m}^{(2)}\psi_{xk_1m}-\frac{l_0^2}{4}a_{66}\left[\frac{\lambda}{\eta_2}\sum_{n=1}^{N}\sum_{m=1}^{M}C_{k_1n}^{(1)}C_{k_2m}^{(2)}w_{nm}+\frac{1}{\eta_1}\sum_{n=1}^{N}C_{k_1n}^{(3)}w_{nk_2}-4\lambda^2\sum_{m=1}^{M}C_{k_2m}^{(3)}\psi_{xk_1m}\right.\\
&\left.+3\lambda\sum_{n=1}^{N}\sum_{m=1}^{M}C_{k_1n}^{(1)}C_{k_2m}^{(1)}\psi_{ynm}-\sum_{n=1}^{N}C_{k_1n}^{(2)}\psi_{xnk_2}\right]+\frac{l_0^2}{4}d_{66}\left[\frac{1}{\eta_1\eta_2}\sum_{n=1}^{N}\sum_{m=1}^{M}C_{k_1n}^{(3)}C_{k_2m}^{(1)}\psi_{ynm}\right.\\
&\left.+\frac{\lambda}{\eta_2^2}\sum_{n=1}^{N}\sum_{m=1}^{M}C_{k_1n}^{(1)}C_{k_2m}^{(3)}\psi_{ynm}-\frac{1}{\eta_2^2}\sum_{n=1}^{N}\sum_{m=1}^{M}C_{k_1n}^{(2)}C_{k_2m}^{(2)}\psi_{xnm}-\frac{\lambda^2}{\eta_2^2}\sum_{m=1}^{M}C_{k_2m}^{(4)}\psi_{xk_1m}\right]=\bar{I}_3\ddot{\psi}_{xk_1k_2}.
\end{aligned}
\tag{47}
$$

The discrete boundary conditions are given by

$$
w_{k_1k_2}=\sum_{n=1}^{N}C_{k_1n}^{(1)}w_{nk_2}=\psi_{xk_1k_2}=\sum_{n=1}^{N}C_{k_1n}^{(1)}\psi_{xnk_2}=\psi_{yk_1k_2}=\sum_{n=1}^{N}C_{k_1n}^{(1)}\psi_{ynk_2}=0,\ \text{at } k_1=1,N,
\tag{48a}
$$

$$
w_{k_1k_2}=\sum_{m=1}^{M}C_{k_2m}^{(1)}w_{mk_1}=\psi_{xk_1k_2}=\sum_{m=1}^{M}C_{k_2m}^{(1)}\psi_{xmk_1}=\psi_{yk_1k_2}=\sum_{m=1}^{M}C_{k_2m}^{(1)}\psi_{ymk_1}=0,\ \text{at } k_2=1,M,
\tag{48b}
$$

for CCCC microplates, the discrete boundary conditions are

$$
w_{k_1k_2}=\psi_{yk_1k_2}=0,\ d_{11}\sum_{n=1}^{N}C_{k_1n}^{(1)}\psi_{xnk_2}+\lambda d_{12}\sum_{m=1}^{M}C_{k_2m}^{(1)}\psi_{ymk_1}=0,\ \text{at } k_1=1,N,
\tag{49a}
$$

$$
w_{k_1k_2}=\psi_{xk_1k_2}=0,\ d_{11}\lambda\sum_{m=1}^{M}C_{k_2m}^{(1)}\psi_{ymk_1}+d_{12}\sum_{n=1}^{N}C_{k_1n}^{(1)}\psi_{xnk_2}=0,\ \text{at } k_2=1,M,
\tag{49b}
$$

$$
\begin{aligned}
&\lambda^2\sum_{m=1}^{M}C_{k_2m}^{(2)}w_{mk_1}-\sum_{n=1}^{N}C_{k_1n}^{(2)}w_{nk_2}+\eta_1\sum_{n=1}^{N}C_{k_1n}^{(1)}\psi_{xnk_2}-\lambda\eta_1\sum_{m=1}^{M}C_{k_2m}^{(1)}\psi_{ymk_1}=0,\\
&\sum_{n=1}^{N}C_{k_1n}^{(2)}\psi_{ynk_2}-\lambda\sum_{n=1}^{N}\sum_{m=1}^{M}C_{k_2m}^{(1)}C_{k_1n}^{(1)}\psi_{xnm}=0,\\
&\sum_{n=1}^{N}\sum_{m=1}^{M}C_{k_2m}^{(1)}C_{k_1n}^{(1)}\psi_{ynm}-\lambda\sum_{m=1}^{M}C_{k_2m}^{(1)}\psi_{xmk_1}=0,\ \text{at } k_1=1,N,\ k_2=1,M,
\end{aligned}
\tag{49c}
$$

for SSSS microplates. The matrix form of Equations (45)-(49) are expressed as

$$
\mathbf{G}\mathbf{b}+\mu_f\mathbf{C}_{\text{vis}}\dot{\mathbf{b}}+\left(\mathbf{M}+\mathbf{M}_{\text{add}}\right)\ddot{\mathbf{b}}=\mathbf{0},
\tag{50}
$$

where $\mathbf{G}$, $\mathbf{C}_{\text{vis}}$, $\mathbf{M}$, and $\mathbf{M}_{\text{add}}$ are $3NM\times 3NM$ matrixes, which represent the stiffness, damping, mass, and added mass, respectively.

The unknown vector $\mathbf{b}$ is assumed as

$$\mathbf{b}=\left\{\left\{w_{k_{12}}\right\}^{\mathrm{T}},\left\{\psi_{xk_{12}}\right\}^{\mathrm{T}},\ \left\{\psi_{yk_{12}}\right\}^{\mathrm{T}}\right\}^{\mathrm{T}}, \tag{51}$$

where $k_{12}=M\times\left(k_1-1\right)+k_2$, $k_{12}=1,\ 2,\ \ldots,N\times M$. The mode shape of vibration is assumed in the form of the decaying exponential function $\mathbf{b}=\mathbf{b}^{*}\mathrm{e}^{-\Omega t}$, where $\Omega = \Omega_r + \mathrm{i}\Omega_i$ is the complex parameter. Ω_r = Re(Ω), namely the damping characteristic coefficient, is the exponentially decaying rate of the unknown vector function **b**; Ω_i = |Im(Ω)| gives the natural angular frequency of the microplate. The symbols Re and Im denote the real and imaginary parts, respectively.

Then, Equation (50) can be rewritten as

$$\left[\mathbf{G}-\omega^2\left(\mathbf{M}+\mathbf{M}_{\mathrm{add}}-\overline{\mu}_f\mathbf{C}_{\mathrm{vis}}\right)\right]\mathbf{b}^{*}=0, \tag{52}$$

where the parameter $\overline{\mu}_f$ is defined in terms of the non-dimensional complex parameter ω, which is similar with the definition of Reynold number in Sader [48]. Equation (52) is solved using an iterative procedure as follows. The iterative steps are:

(i) With the assumption of $\overline{\mu}_f=0$, the complex parameter ω is calculated from $\mathbf{G}-\omega^2\left[\mathbf{M}+\mathbf{M}_{\mathrm{add}}\right]=0$;

(ii) Using ω obtained in step (i), $\overline{\mu}_f$ is determined by Equation (35c), and ω is updated by Equation (52);

(iii) Repeat step (ii) if the relative error is more than 0.1% between two consecutive iterations.

3. Numerical results

Several numerical examples are performed to study the free vibration of FGM microplates in contact with viscous fluid. The influences of related parameters, such as the aspect ratio, gradient index, fluid height, size parameter, fluid density, fluid viscosity, and slenderness ratio are investigated in detail. The material constants of the bottom surface made from SUS304 are elastic modulus E_m = 207.78 GPa, Poisson's ratio υ_m = 0.3177, mass density ρ_m = 8166 kg/m^3, while the material constants of the top surface made from Si_3N_4 are elastic modulus E_c = 322.27 GPa, Poisson's ratio υ_c = 0.24, mass density ρ_c = 2370 kg/m^3. Unless otherwise stated, physical parameters are taken as: the length L_x, width L_y and thickness h_0 of microplates as 10×10×1 μm, gradient index n = 1, size parameter l = 1 μm, fluid depth h_f = 10 μm and fluid density ρ_f = 1000 kg/m^3. The fundamental frequency $f = \Omega_i/2\pi$ and the damping characteristic coefficient Ω_r for the free vibration of CCCC and SSSS FGM microplates are discussed in following numerical examples.

3.1. Model validation

Table 1 demonstrates the convergence of the complex parameter Ω for the FGM microplates in viscous fluid with the viscosity μ_f = 1 Pa·s. The values of complex parameter $\Omega = \Omega_r + \mathrm{i}\Omega_i$ are listed with different discrete points N and M. Clearly, the complex parameter Ω is convergent with the increasing N and M for both CCCC and SSSS microplates. To achieve the accuracy, $N = M$ = 24 and 10 are adopted for CCCC and SSSS microplates, respectively.

Table 2 presents the fundamental frequency $\mathrm{Im}\left(\Omega(L_x^2 / h_0)\sqrt{\rho / E}\right)$ of size-dependent Si_3N_4 microplates without the fluid. Yin et al. [21] obtained the analytical results for the Kirchhoff microplate based on the MCST. The comparison between two results shows a good consistence.

Table 3 provides the normalized fundamental frequency $\mathrm{Im}\left[\Omega h_0\sqrt{\rho/\left(E/2(1+\nu)\right)}\right]$ of SSSS nanoplates in different fluid environments when $L_x = L_y = h_f$ = 10 nm, n = 0, l = 0, υ = 0.3. Four common fluid media are considered: air (ρ_f = 1.2 kg/m^3, μ_f =16.5×10^{-6} Pa·s), vacuum (without fluid effect), water (ρ_f = 1000 kg/m^3, μ_f =8.9×10^{-4} Pa·s) and honey (ρ_f = 1420 kg/m^3, μ_f =10 Pa·s). Hosseini-Hashemi et al. [53] calculated the frequency of Kirchhoff nano-plates in different fluid environments. Again, the present results are verified by the Hosseini-Hashemi et al.'s results.

3.2. Fundamental frequency

Figure 2 displays the effect of the size parameters h_0 / l on the frequency (f) ~ viscosity (μ_f) curves of CCCC and SSSS FGM microplates. The fundamental frequencies of CCCC and SSSS microplates decrease as the size parameter enlarges at a given fluid viscosity. As the fluid viscosity increases, the fundamental frequencies first decrease slightly, next decrease rapidly at a small interval, and then reduce to zero slowly. The small interval is regarded as the sensitive viscosity interval where the frequency decays sharply. In the sensitive viscosity interval, the frequency of CCCC microplates decays more sharply than that of SSSS microplates. Corresponding to h_0 / l=1, 2, 5, and 10, the sensitive viscosity intervals are about [7.5, 8.7] Pa·s, [5, 6] Pa·s, [3.6, 4.5] Pa·s, and [3.4, 4.2] Pa·s for CCCC microplates, and about [7, 9] Pa·s, [4.3, 6] Pa·s, [3.2, 4.5] Pa·s, and [3, 4] Pa·s for SSSS microplates. Clearly, the sensitive viscosity interval is shifted to the left with the increase of the size parameter. The results indicate that the viscous damping effect of fluids can reduce the fundamental frequency, and a large enough fluid viscosity can suppress the vibration of the structure.

Figure 3 discusses the effect of the gradient index n on the frequency ~ viscosity curves of CCCC and SSSS FGM microplates. The fundamental frequencies decrease as the gradient index enlarges at a given fluid viscosity for CCCC and SSSS FGM microplates. The gradient index has a minor effect on the sensitivity viscosity interval. It can be seen that all sensitivity viscosity intervals are kept at the range of [7, 9] Pa·s for CCCC and SSSS microplates approximately.

Figure 4 examines the influence of the fluid height h_f / h_0 on the frequency ~ viscosity curves of CCCC and SSSS FGM microplates. Notice that h_f / h_0 = 0 implies no fluid effect. At this case, the frequency is a constant with the change of the viscosity. The fundamental frequencies of CCCC and SSSS microplates decrease as the fluid height enlarges at a given fluid viscosity. The sensitive viscosity interval is shifted to left with the increase of the fluid height.

Figure 5 examines the effect of the fluid density ρ_f on the frequency ~ viscosity curves of CCCC and SSSS FGM microplates. Four different fluid media are selected as: bromoform, honey, water and acetone with densities of 2820 kg/m^3, 1420 kg/m^3, 1000 kg/m^3 and 788 kg/m^3, respectively. The fundamental frequency of CCCC and SSSS microplates decrease as the fluid density enlarges when $\mu_f \in$ [0, 6] Pa·s, while the influence of the fluid density is unobvious when μ_f >13 Pa·s. Clearly, the sensitive viscosity interval is shifted to the right with the increase of the fluid density. As for the CCCC microplate, the sensitive viscosity interval is about [7, 8] Pa·s when ρ_f = 788 kg/m^3, while it increases to [11.5, 13] Pa·s when ρ_f = 2820 kg/m^3. The sensitive viscosity interval of the SSSS microplate is about [6.5, 8.5] Pa·s when ρ_f = 788 kg/m^3, and [10.5, 13] Pa·s when ρ_f = 2820 kg/m^3.

Figure 6 shows the effect of the aspect ratio L_x / L_y on the frequency ~ viscosity curves of CCCC and SSSS FGM microplates. The frequencies of CCCC and SSSS microplates decrease as the aspect ratio reduces at a given fluid viscosity when $\mu_f \in$ [0, 6] Pa·s. With the increase of aspect ratio, the sensitive viscosity interval is shifted to the left for the CCCC FGM microplate, whereas it is slightly affected for the SSSS FGM microplate.

Figure 7 plots the effect of the slenderness ratio L_x / h_0 on the frequency ~ viscosity curves of CCCC and SSSS FGM microplates. The frequencies of CCCC and SSSS microplates decrease as the slenderness ratio enlarges at a given fluid viscosity. In particular, the sensitive viscosity interval is sensitive to the slenderness ratio, and it is shifted to the left as the slenderness ratio increases.

3.3. Damping characteristic coefficient

Figure 8 gives the effect of the size parameter h_0 / l on the damping characteristic coefficient (Ω_r) ~ viscosity (μ_f) curves of CCCC and SSSS FGM microplates. Interestingly, there is a critical viscosity μ_{f0} corresponding to the peak of Ω_r. As the fluid viscosity increases, the damping characteristic coefficient enlarges when $\mu_f < \mu_{f0}$, but it decreases when $\mu_f > \mu_{f0}$. The effect of the size parameter on Ω_r is significant when μ_f > 3. As the size parameter enlarges, the peak of Ω_r and the critical viscosity decrease rapidly. However, when μ_f > 8, the damping characteristic coefficient increases with the decrease of size parameter.

The effect of the gradient index n on the damping characteristic coefficient ~ viscosity

curves of CCCC and SSSS FGM microplates is plotted in Figure 9. A large gradient index leads to a reduction of Ω_r and its peak for a given fluid viscosity. The variation of the critical viscosity on the gradient index is unobvious.

Figure 10 analyzes the effect of the fluid height h_f / h_0 on the damping characteristic coefficient ~ viscosity curves of CCCC and SSSS FGM microplates. As the fluid height increases, the peak of Ω_r and critical viscosity increase markedly. For both CCCC and SSSS FGM microplates, the damping characteristic coefficient increases with the larger fluid height when $\mu_f < 5$, but it has a decrease trend when $\mu_f > 12$.

The effect of the fluid density ρ_f on the damping characteristic coefficient ~ viscosity curves of CCCC and SSSS FGM microplates is shown in Figure 11. For a smaller fluid density, the peak of Ω_r has a larger value and the critical viscosity has a smaller value. The damping characteristic coefficient reduces as the fluid density increases when $\mu_f < 7$, but it has an opposite trend when $\mu_f > 13$.

Figure 12 gives the effect of the aspect ratio L_x / L_y on the damping characteristic coefficient ~ viscosity curves of CCCC and SSSS FGM microplates. As the aspect ratio enlarges, the peak of Ω_r increases, while the critical viscosity μ_{f0} reduces. The damping characteristic coefficient of CCCC and SSSS FGM microplates increases as the aspect ratio is enlarged at a given fluid viscosity.

Figure 13 shows the effect of the slenderness ratio L_x / h_0 on the damping characteristic coefficient ~ viscosity curves of CCCC and SSSS FGM microplates. The damping characteristic coefficient enlarges slightly as the fluid viscosity increases when $\mu_f <3$, but it has an opposite trend when $\mu_f >8$. For a smaller slenderness ratio, the peak of Ω_r reaches a larger value at the higher critical viscosity.

4. Conclusions

In this work, the free vibration for size-dependent FGM Mindlin microplates in contact with viscous fluid is conducted based on the MCST. The Mori-Tanaka method is applied for predicting the gradient variation of FGM microplates. The introduction of a physical neutral plane simplifies the microplate model because it can exclude the stretching-bending coupling effect. The hydrodynamic loading on the FGM microplate including both the inertial effect and viscous damping effect is taken into account based on the Navier-Stokes equation. The microplate-fluid coupling equations are established based on the Hamilton's principle, and numerically solved using the DQ method. The influences of the gradient index, aspect ratio, fluid depth, slenderness ratio, fluid viscosity, fluid density, size parameter, and boundary condition on vibration characteristics are considered. It is concluded that:

(1) There is a sensitive viscosity interval where the frequency decays sharply.

(2) The viscous damping effect can reduce the fundamental frequency, and a large enough fluid viscosity can suppress the vibration of the structure.

(3) The frequencies of CCCC and SSSS microplates decrease markedly as the slenderness ratio, fluid height, size parameter, and gradient index increase.

(4) There is a critical viscosity μ_{f0} corresponding to the peak of the damping characteristic coefficient. As the fluid viscosity increases, the damping characteristic coefficient enlarges when $\mu_f < \mu_{f0}$, but it decreases when $\mu_f > \mu_{f0}$.

(5) The critical viscosity μ_{f0} reduces as the slenderness ratio, aspect ratio, and size parameters enlarge.

Acknowledgement

The support from the National Natural Science Foundation of China under Grant [numbers 11725207 and 12021002] is acknowledged.

Disclosure statement

No potential conflict of interest was reported by the author(s).

References

[1] Suresh S, Mortensen A. Fundamentals of Functionally Graded Materials: Processing and Thermomechanical Behavior of Graded Metals and Metal-Ceramic Composites. London: IOM Communications Ltd; 1998.

[2] Joshi PV, Gupta A, Jain NK, et al. Effect of thermal environment on free vibration and buckling of partially cracked isotropic and FGM micro plates based on a non classical Kirchhoff's plate theory: An analytical approach. *Int J Mech Sci*. 2017;131:155–170.

[3] Akgoz B, Civalek O. Free vibration analysis of axially functionally graded tapered Bernoulli-Euler microbeams based on the modified couple stress theory. *Compos Struct*. 2013;98:314–322.

[4] Rad AB, Shariyat M. Thermo-magneto-elasticity analysis of variable thickness annular FGM plates with asymmetric shear and normal loads and non-uniform elastic foundations. *Arch Civ Mech Eng*. 2016;16:448–466.

[5] Kiani Y, Eslami MR. Thermal postbuckling of imperfect circular functionally graded material plates: examination of Voigt, Mori-Tanaka, and Self-Consistent schemes. *J Press Vessel Technol*. 2015;137:021201.

[6] Jin ZH, Paulino GH, Dodds RH. Finite element investigation of quasi-static crack growth in functionally graded materials using a novel cohesive zone fracture model. *J Appl Mech*. 2002;69(3):370–379.

[7] Shen HS, Wang ZX. Assessment of Voigt and Mori-Tanaka models for vibration analysis of functionally graded plates. *Compos Struct*. 2012;94:2197–2208.

[8] Firoozbakhsh K, Ahmadian MT, Rahaeifard M, et al. A novel device for detection of soft tissue inflammation: dynamic behaviour of a functionally graded AFM cantilever. *Int J Exp Comput. Biomech*. 2012;2:1–9.

[9] Witvrouw A, Mehta A. The use of functionally graded poly-SiGe layers for MEMS applications. *Mater Sci Forum.* 2005;492:255–60.

[10] Lam DCC, Yang F, Chong ACM, et al. Experiments and theory in strain gradient elasticity. *J Mech Phys Solids*. 2003;51:1477–1508.

[11] Malekzadeh P, Shojaee M. Free vibration of nanoplates based on a nonlocal two-variable refined plate theory. *Compos Struct.* 2013;95:443–452.

[12] Eltaher MA, Omar FA, Abdalla WS, et al. Bending and vibrational behaviors of piezoelectric nonlocal nanobeam including surface elasticity. *Wave Random Complex*. 2018;29(2):264–280.

[13] Mindlin RD, Tiersten HF. Effects of couple-stresses in linear elasticity. *Arch Ration Mech Anal*. 1962;11:415–448.

[14] Toupin RA. Elastic materials with couple-stresses. *Arch Ration Mech Anal.* 1962;11:385–414.

[15] Babu B, Patel BP. On the finite element formulation for second-order strain gradient nonlocal beam theories. *Mech Adv Mater Struct.* 2019;26:1316–1332.

[16] Khorshidi MA, Shariati M. An investigation of stress wave propagation in a shear deformable nanobeam based on modified couple stress theory. *Wave Random Complex*. 2016;26(2):243–258.

[17] Şimşek M, Reddy JN. Bending and vibration of functionally graded microbeams using a new higher order beam theory and the modified couple stress theory. *Int J Eng Sci*. 2013;64:37–53.

[18] Reddy JN. Microstructure-dependent couple stress theories of functionally graded beams. *J Mech Phys Solids*. 2011;59:2382–2399.

[19] Nateghi A, Salamat-talab M, Rezapour J, et al. Size dependent buckling analysis of functionally graded micro beams based on modified couple stress theory. *Appl Math Model.* 2012;36:4971–4987.

[20] Yang F, Chong ACM, Lam DCC, et al. Couple stress based strain gradient theory for elasticity. *Int J Solids Struct*. 2002;39:2731–2743.

[21] Yin L, Qian Q, Wang L, et al. Vibration analysis of microscale plates based on modified couple stress theory. *Acta Mech Solida Sin.* 2010;23:387–393.

[22] Mirsalehi M, Azhari M, Amoushahi H. Stability of thin FGM microplate subjected to mechanical and thermal loading based on the modified couple stress theory and spline finite

strip method. *Aeros Sci Technol*. 2016;47:356–366.
[23] Hajmohammad MH, Zarei MS, Sepehr M, et al. Bending and buckling analysis of functionally graded annular microplate integrated with piezoelectric layers based on layerwise theory using DQM. *Aeros Sci Technol*. 2018;79:679–688.
[24] Guo L, Xin XY, Shahsavari D, et al. Dynamic response of porous E-FGM thick microplate resting on elastic foundation subjected to moving load with acceleration. *Thin-Walled Struct*. 2022;73:108981.
[25] Guo HL, He TH, Tian XG, et al. Size-dependent mechanical-diffusion responses of multilayered composite nanoplates. *Wave Random Complex*. 2021;31(6):2355–2384.
[26] Akbaş ŞD. Free vibration of edge cracked functionally graded microscale beams based on the modified couple stress theory. *Int J Struct Stab Dyn*. 2017;17:1750033.
[27] Li YS, Pan E. Static bending and free vibration of a functionally graded piezoelectric microplate based on the modified couple-stress theory. *Int J Eng Sci*. 2015;97:40–59.
[28] Ke LL, Yang J, Kitipornchai S, et al. Bending, buckling and vibration of size-dependent functionally graded annular microplates. *Compos Struct*. 2012;94:3250–3257.
[29] Ke LL, Wang YS, Yang J, et al. Free vibration of size-dependent Mindlin microplates based on the modified couple stress theory. *J Sound Vib*. 2012;331:94–106.
[30] Ma YL, Gao YH, Yang WL, et al. Free vibration of a micro-scale composite laminated Reddy plate using a finite element method based on the new modified couple stress theory. *Results Phys*. 2019;16:102903.
[31] Shabani R, Sharafkhani N, Tariverdilo S, et al. Dynamic analysis of an electrostatically actuated circular micro-plate interacting with compressible fluid. *Acta Mech*. 2013;224:2025–2035.
[32] Omiddezyani S, Jafari-Talookolaei RA, Abedi M, et al. The size-dependent free vibration analysis of a rectangular Mindlin microplate coupled with fluid. *Ocean Eng*. 2018;163:617–629.
[33] Ramian A, Jafari-Talookolaei RA, Valvo PS, et al. Free vibration analysis of sandwich plates with compressible core in contact with fluid. *Thin-Walled Struct*. 2020;157:107088.
[34] Chiba M, Abet K. Nonlinear hydroelastic vibration of a cylindrical tank with an elastic bottom containing liquid-analysis using harmonic balance method. *Thin-Walled Struct*. 1999;34:233–260.
[35] Rahman M, Bhatta DD. Evaluation of added mass and damping coefficient of an oscillating circular cylinder. *Appl Math Model*. 1993;17:70–79.
[36] Wu HY, Zhou SJ. Vibration of sensor diaphragm with residual stress coupled with liquids: effect of the residual stress. *Sens Rev*. 2014;34:110–116.
[37] Liao CY, Ma CC. Vibration characteristics of rectangular plate in compressible inviscid fluid. *J Sound Vib*. 2016;362:228–251.
[38] Lu HC, Wu SF. Reconstruction of vibroacoustic responses of a highly nonspherical

structure using Helmholtz equation least-squares method. *J Acoust Soc Am*. 2009;125:1538–1548.

[39] Graham WR. Analytical approximations for the modal acoustic impedances of simply supported, rectangular plates. *J Acoust Soc Am.* 2007;122(2):719–730.

[40] Qiu LC. Modeling and simulation of transient responses of a flexible beam floating in finite depth water under moving loads. *Appl Math Model*. 2009;33:1620–1632.

[41] Ostasevicius V, Dauksevicius R, Gaidys R, et al. Numerical analysis of fluid-structure interaction effects on vibrations of cantilever microstructure. *J Sound Vib*. 2007;308:660–673.

[42] Kozlovsky Y. Vibration of plates in contact with viscous fluid: Extension of Lamb's model. *J Sound Vib*. 2009;326:332–339.

[43] Atkinson C, Lara MMD. The frequency response of a rectangular cantilever plate vibrating in a viscous fluid. *J Sound Vib*. 2007;300:352–367.

[44] Vancura C, Dufour I, Heinrich SM, et al. Analysis of resonating microcantilevers operating in a viscous liquid environment. *Sensor Actuator A Phys*. 2008;141:43–51.

[45] Abassi W, Baroudi AE, Razafimahery F. Vibration analysis of Euler-Bernoulli beams partially immersed in a viscous fluid. *Phys Res Int*. 2016;2016:6761372.

[46] Tuck EO. Calculation of unsteady flows due to small motions of cylinders in a viscous fluid. *J Eng Math*. 1969;3:29–44.

[47] Sader JE. Frequency response of cantilever beams immersed in viscous fluids with applications to the atomic force microscope. *J Appl Phys*. 1998;84:64–76.

[48] Chon JWM, Mulvaney P, Sader JE. Experimental validation of theoretical models for the frequency response of atomic force microscope cantilever beams immersed in fluids. *J Appl Phys*. 2000;87:3978–3988.

[49] Green CP, Sader JE. Frequency response of cantilever beams immersed in viscous fluids near a solid surface with applications to the atomic force microscope. *J Appl Phys* 2005;98:114913.

[50] Golzar FG, Shabani R, Hatami H, et al. Dynamic Response of an Electrostatically Actuated Micro-Beam in an Incompressible Viscous Fluid Cavity. *J Microelectromech Syst*. 2014;23:555–562.

[51] Korayem MH, Sharahi HJ. Analysis of the effect of mechanical properties of liquid and geometrical parameters of cantilever on the frequency response function of AFM. *Int J Adv Manuf Technol*. 2011;57:477–489.

[52] Wu ZM, Ma XH. Dynamic analysis of submerged microscale plates: the effects of acoustic radiation and viscous dissipation. *Proc Math Phys Eng Sci*. 2016;472:20150728.

[53] Hosseini-Hashemi S, Arpanahi RA, Rahmanian S, et al. Free vibration analysis of nano-plate in viscous fluid medium using nonlocal elasticity. *Eur J Mech A Solids*. 2019;74:440–448.

[54] Khorshidi K, Karimi M, Bahrami M, et al. Fluid-structure interaction analysis of vibrating

microplates in interaction with sloshing fluids with free surface. *Appl Ocean Res*. 2022;121:103088.

[55] Bakhsheshy A, Mahbadi H. The effect of fluid surface waves on free vibration of functionally graded microplates in interaction with bounded fluid. *Ocean Eng*. 2019;194:106646.

[56] Karimi M, Khorshidi K, Dimitri R, et al. Size-dependent hydroelastic vibration of FG microplates partially in contact with a fluid. *Compos Struct*. 2020;244:112320.

[57] Wang CM, Ke LL, Chowdhury ANR, et al. Critical examination of midplane and neutral plane formulations for vibration analysis of FGM beams. *Eng Struct*. 2017;130:275–281.

[58] Zhang DG, Zhou YH. A theoretical analysis of FGM thin plates based on physical neutral surface. *Comput Mater Sci*. 2009;44:716–720.

[59] Shu C. Differential Quadrature and Its Application in Engineering. Berlin: Springer; 2000.

Table 1. The complex parameter Ω ($\times 10^8$) for CCCC and SSSS FGM microplates in contact with viscous fluid on one side ($L_x = L_y = h_f = 10$ μm, $h_0 = 1$ μm, $\mu_f = 1$ Pa·s, $n = 1$, $l = 1$ μm, $\rho_f = 1000$ kg/m^3).

N, M	CCCC	SSSS
$N = M = 8$	12.362 + 1.0711i	0.54119 + 0.064375i
$N = M = 10$	10.715 + 0.89657i	0.54159 + 0.064380i
$N = M = 12$	10.043 + 0.83242i	0.54159 + 0.064380i
$N = M = 18$	9.4138 + 0.77530i	0.54159+ 0.064380i
$N = M = 22$	9.2872 + 0.76480i	0.54159+ 0.064380i
$N = M = 24$	9.2497 + 0.76183i	0.54159+ 0.064380i
$N = M = 25$	9.2351 + 0.76055i	——

Table 2. The fundamental frequency $\mathrm{Im}\left(\Omega(L_x^2/h)\sqrt{\rho/E}\right)$ for size-dependent Si_3N_4 SSSS microplates with $L_x/h_0=10$.

		l (m)			
		0	0.0005	0.001	0.003
$L_x=0.5$, $L_y=1$ m	present	3.6317	3.6325	3.6342	3.6614
	Yin et al. [21]	3.710	3.711	3.713	3.939
$L_x=L_y=1$ m	present	5.737	5.7373	5.7383	5.7482
	Yin et al. [21]	5.9356	5.9360	5.9369	5.9472

Table 3. The fundamental frequency $\mathrm{Im}\left(\Omega h\sqrt{\rho/\left(E/2(1+\nu)\right)}\right)$ of SSSS nanoplate in different fluid environments ($L_x = L_y = h_f = 10$ m, $n = 0$, $l = 0$, $\upsilon = 0.3$).

		$L_x/h_0 = 10$	$L_x/h_0 = 20$
Air	present	0.09279	0.02374
	Malekzadeh and Shojaee [11]	0.0930	0.0239
	Hosseini-Hashemi et al. [53]	0.0960	0.02396
Vacuum	present	0.0930	0.02386
	Hosseini-Hashemi et al. [53]	0.0963	0.02409
Water	present	0.04068	0.007722
	Hosseini-Hashemi et al. [53]	0.0429	0.007838
Honey	Present	0.035146	0.006583
	Hosseini-Hashemi et al. [53]	0.03690	0.006289
Inviscid Honey	Present	0.03515	0.006583
	Hosseini-Hashemi et al. [53]	0.037153	0.006683

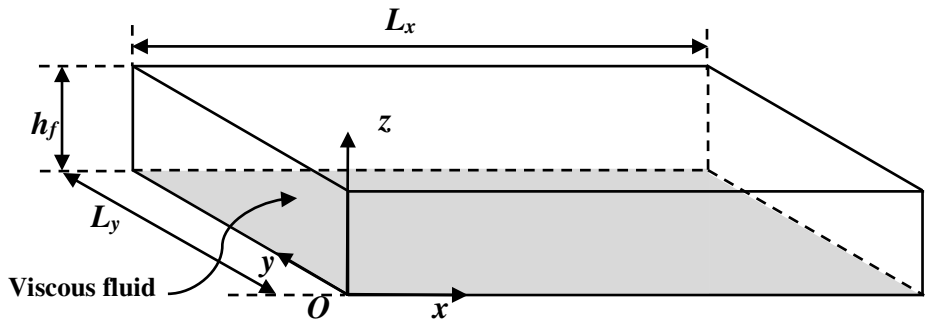

(a) Fluid-plate coupled system

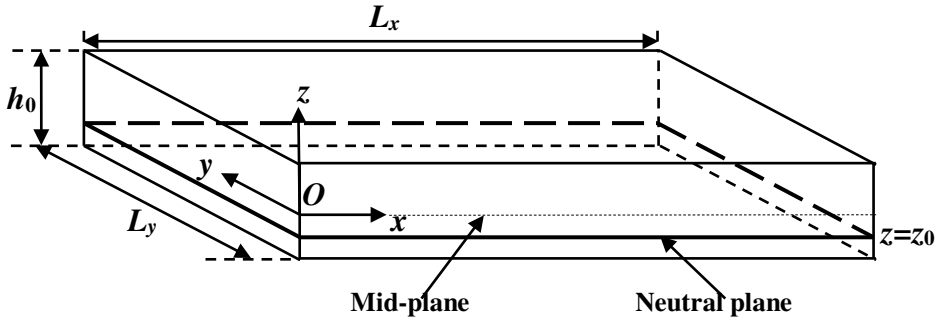

(b) Spatial geometry of microplates

Figure 1. An FGM microplate in viscous fluid: (a) Fluid-plate system and (b) Spatial geometry of microplates.

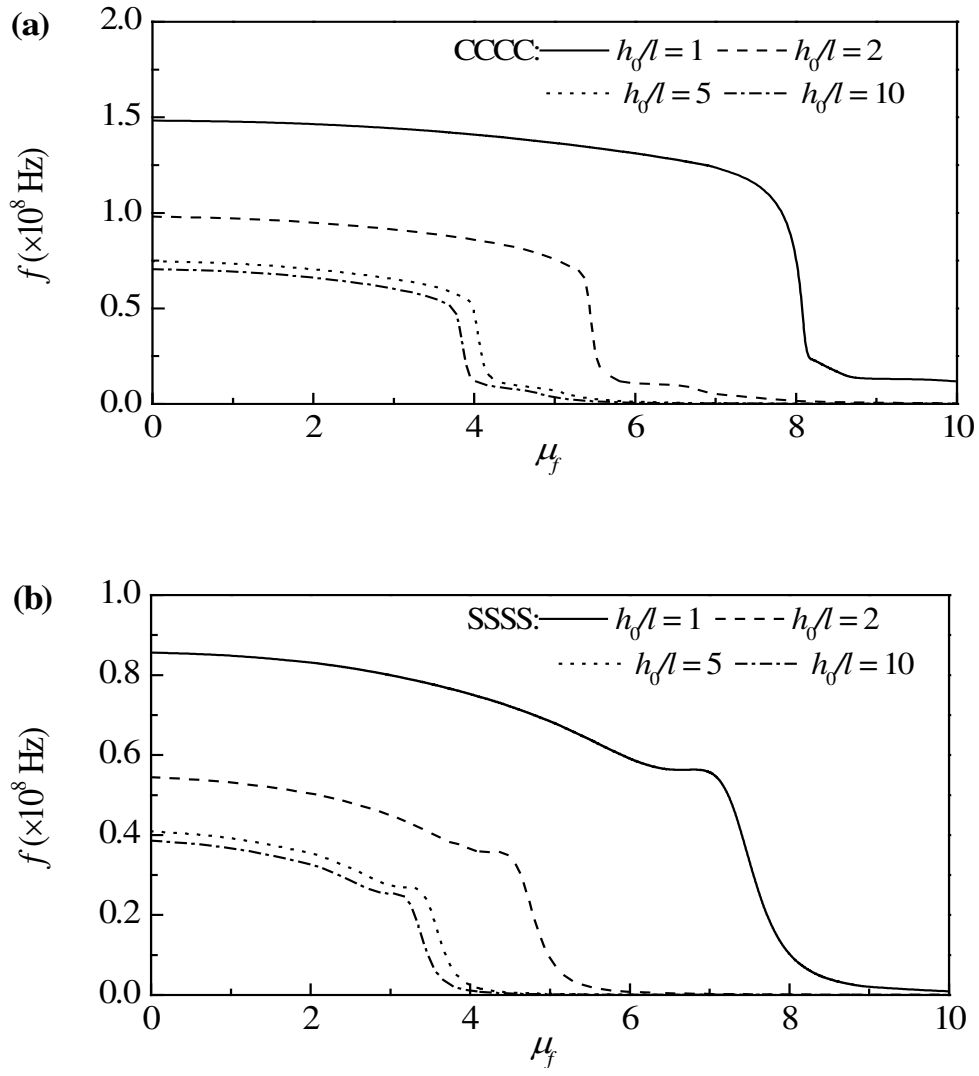

Figure 2. The effect of the size parameters h_0 / l on the frequency ~ viscosity curves of CCCC and SSSS FGM microplates (L_x / L_y = 1, L_x / h_0 = 10, n = 1, h_f / h_0= 10, ρ_f = 1000 kg/m^3): (a) CCCC and (b) SSSS.

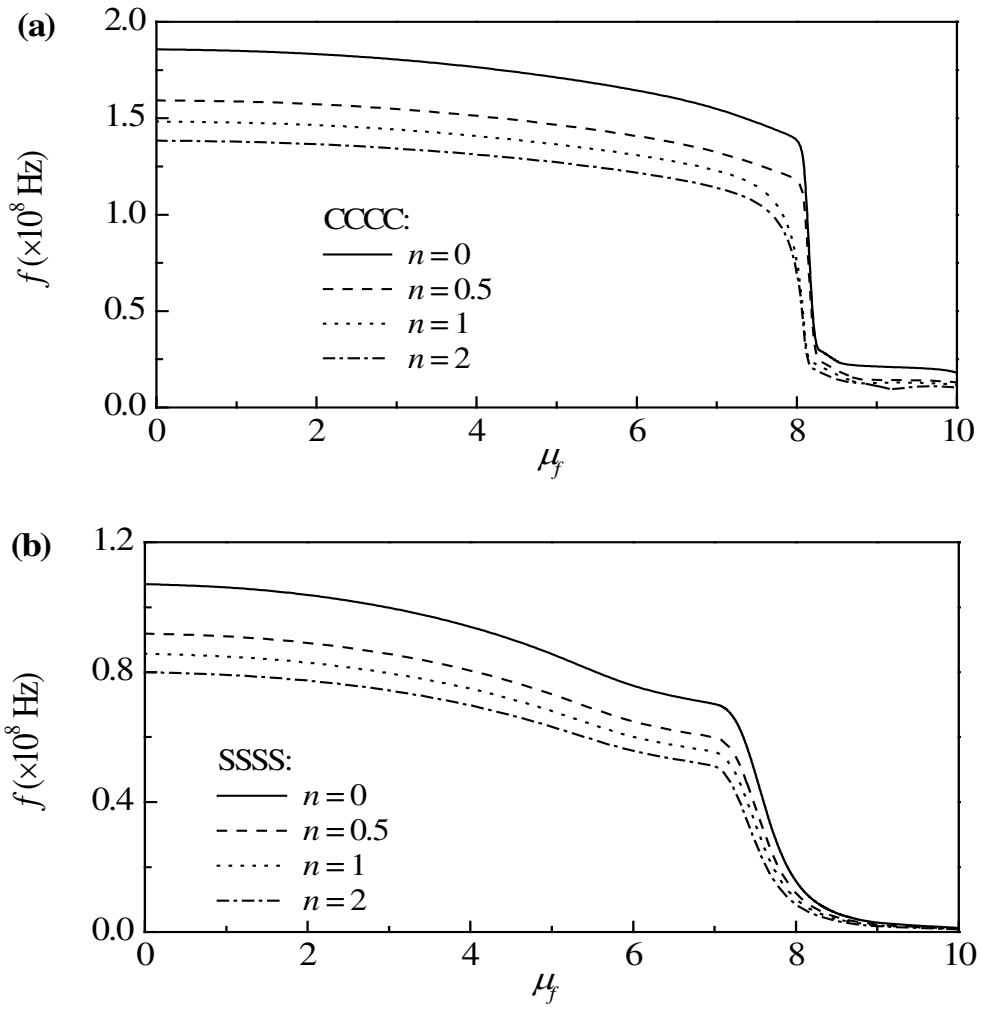

Figure 3. The effect of the gradient index n on the frequency ~ viscosity curves of CCCC and SSSS FGM microplates (L_x / L_y = 1, L_x / h_0 = 10, h_0 / l = 1, h_f / h_0= 10, ρ_f = 1000 kg/m^3): (a) CCCC and (b) SSSS.

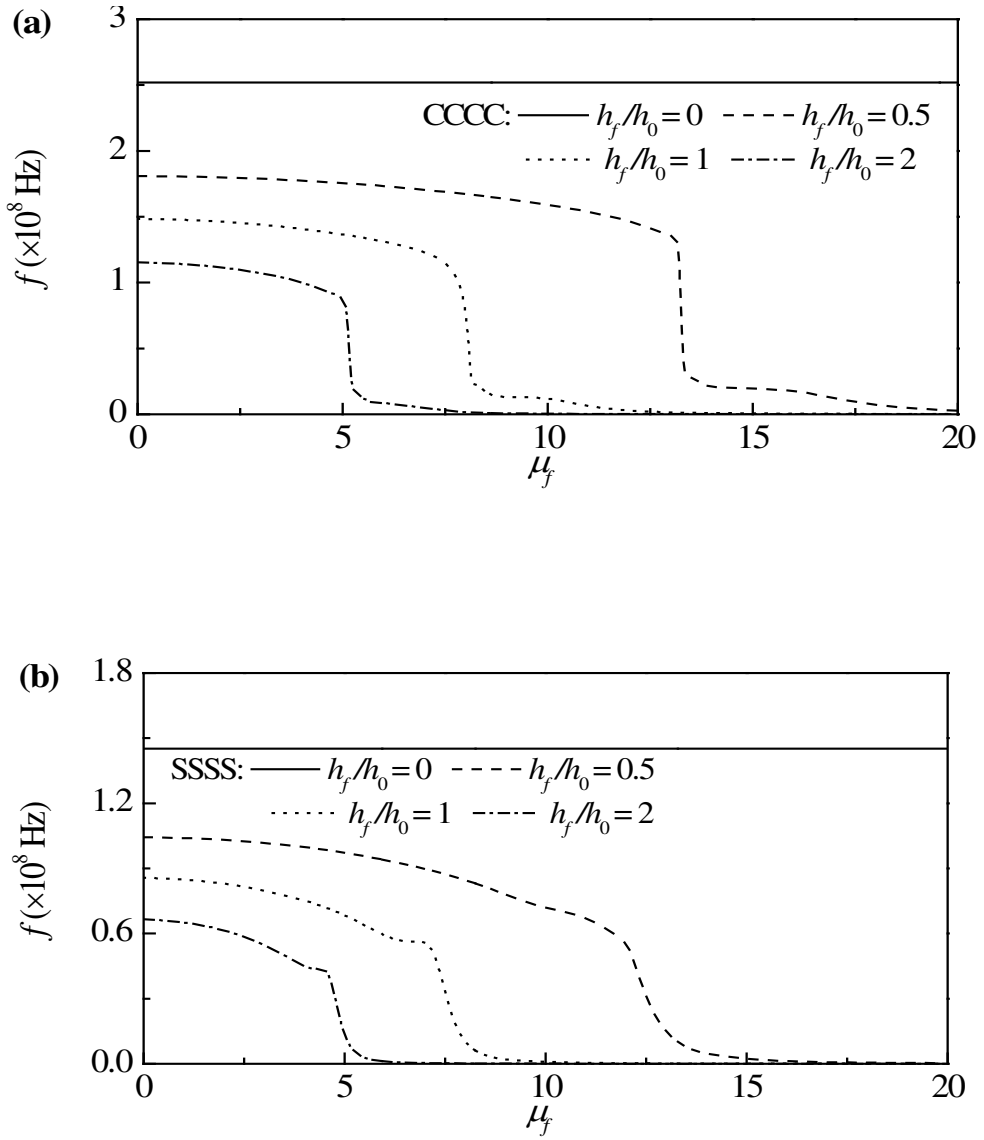

Figure 4. The influence of the fluid height h_f / h_0 on the frequency ~ viscosity curves of CCCC and SSSS FGM microplates (L_x / L_y = 1, L_x / h_0 = 10, n = 1, h_0 / l = 1, ρ_f = 1000 kg/m^3): (a) CCCC and (b) SSSS.

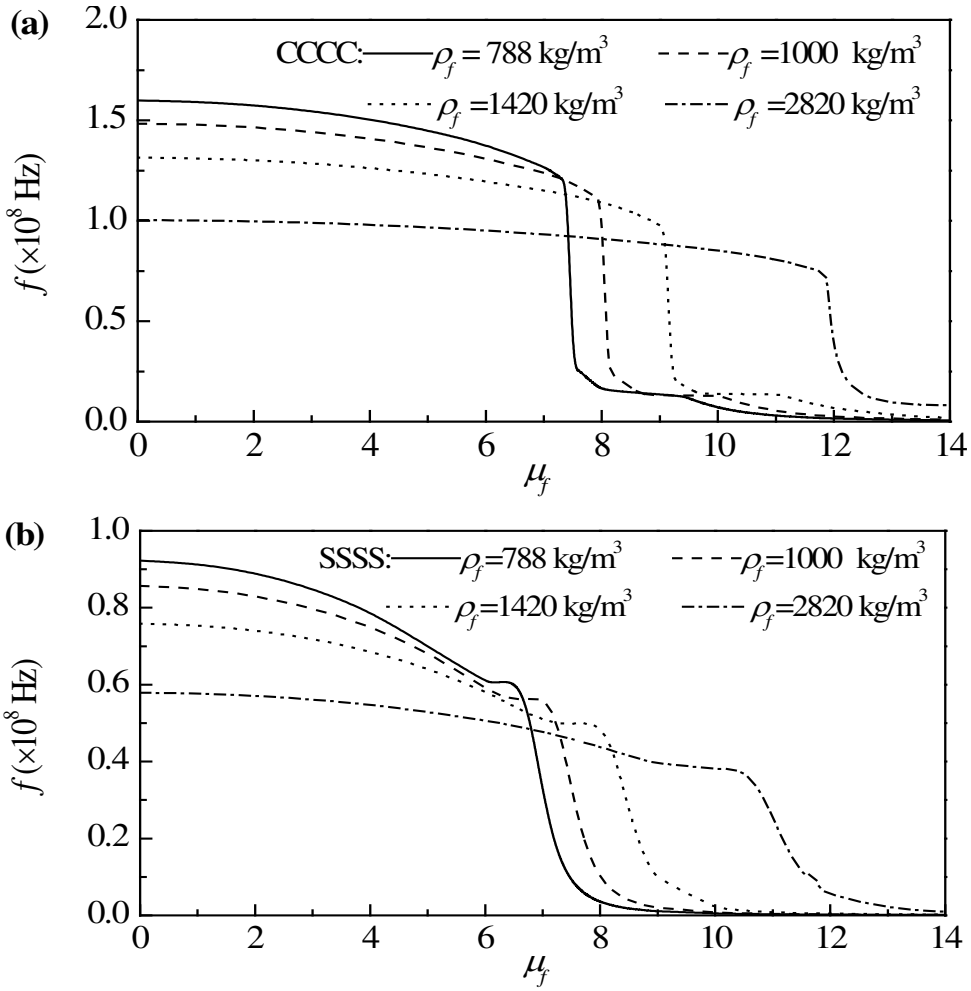

Figure 5. The effect of the fluid density ρ_f on the frequency ~ viscosity curves of CCCC and SSSS FGM microplates (L_x / L_y = 1, L_x / h_0 = 10, n =1, h_0 / l = 1, h_f / h_0= 10): (a) CCCC and (b) SSSS.

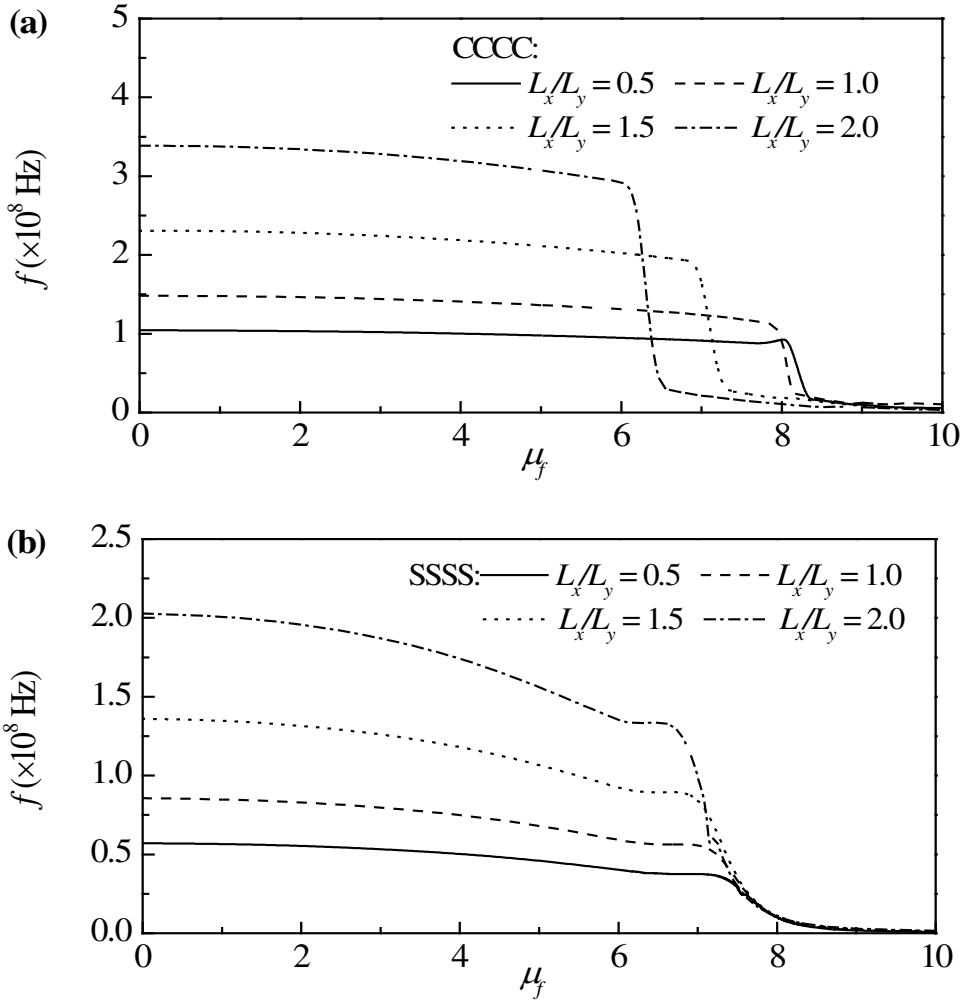

Figure 6. The effect of the aspect ratio L_x / L_y on the frequency ~ viscosity curves of CCCC and SSSS FGM microplates (L_x / h_0 = 10, n = 1, h_0 / l = 1, h_f / h_0= 10, ρ_f = 1000 kg/m^3): (a) CCCC and (b) SSSS.

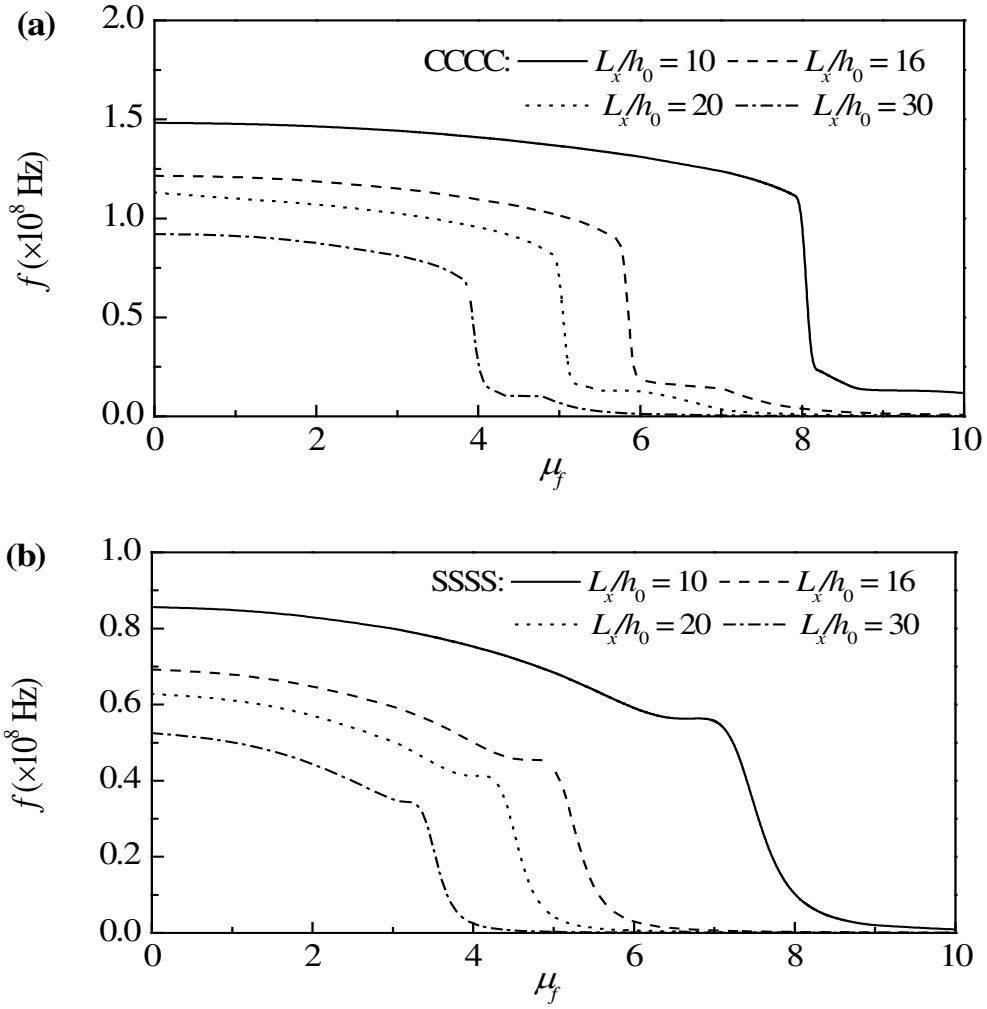

Figure 7. The effect of the slenderness ratio L_x / h_0 on the frequency ~ viscosity curves of CCCC and SSSS FGM microplates (L_x / L_y = 1, n = 1, h_0 / l = 1, h_f / h_0= 10, ρ_f = 1000 kg/m^3): (a) CCCC and (b) SSSS.

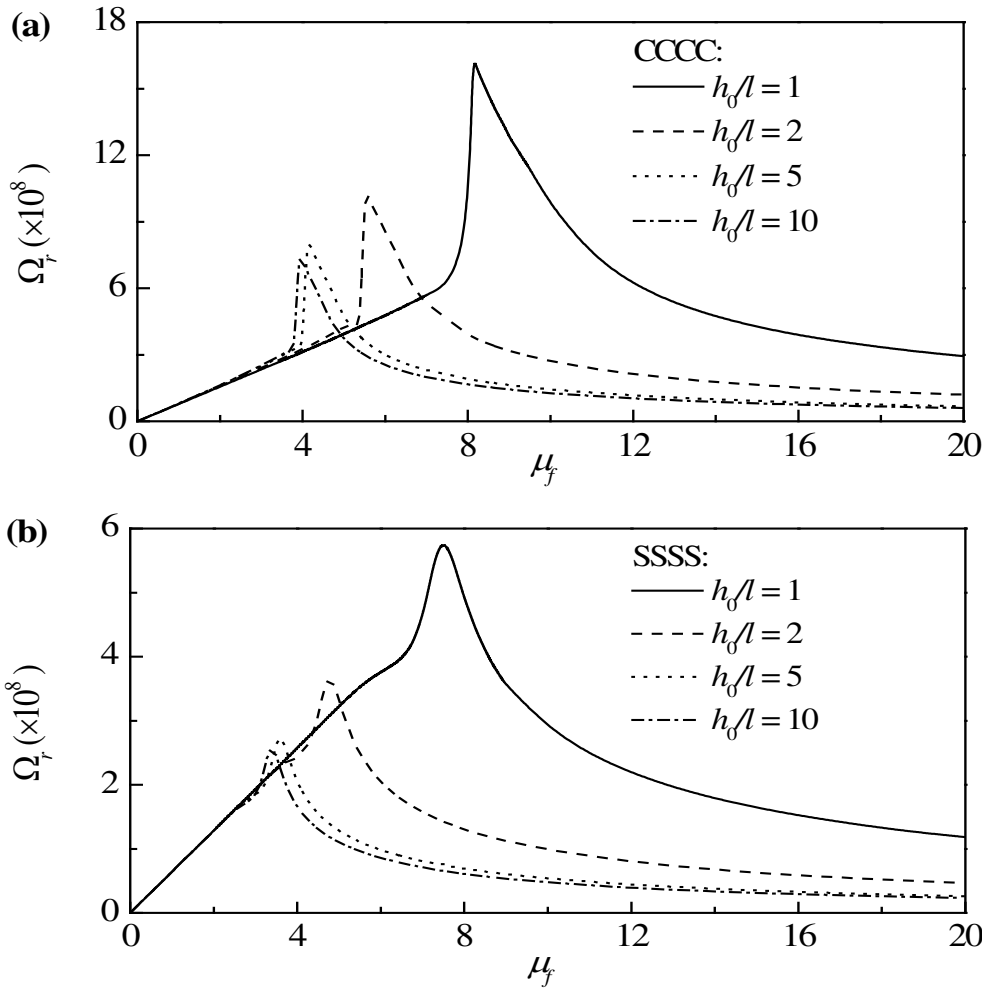

Figure 8. The effect of the size parameters h_0 / l on the damping characteristic coefficient ~ viscosity curves of CCCC and SSSS FGM microplates (L_x / L_y = 10, L_x / h_0 = 10, n = 1, h_f / h_0= 10, ρ_f = 1000 kg/m^3): (a) CCCC and (b) SSSS.

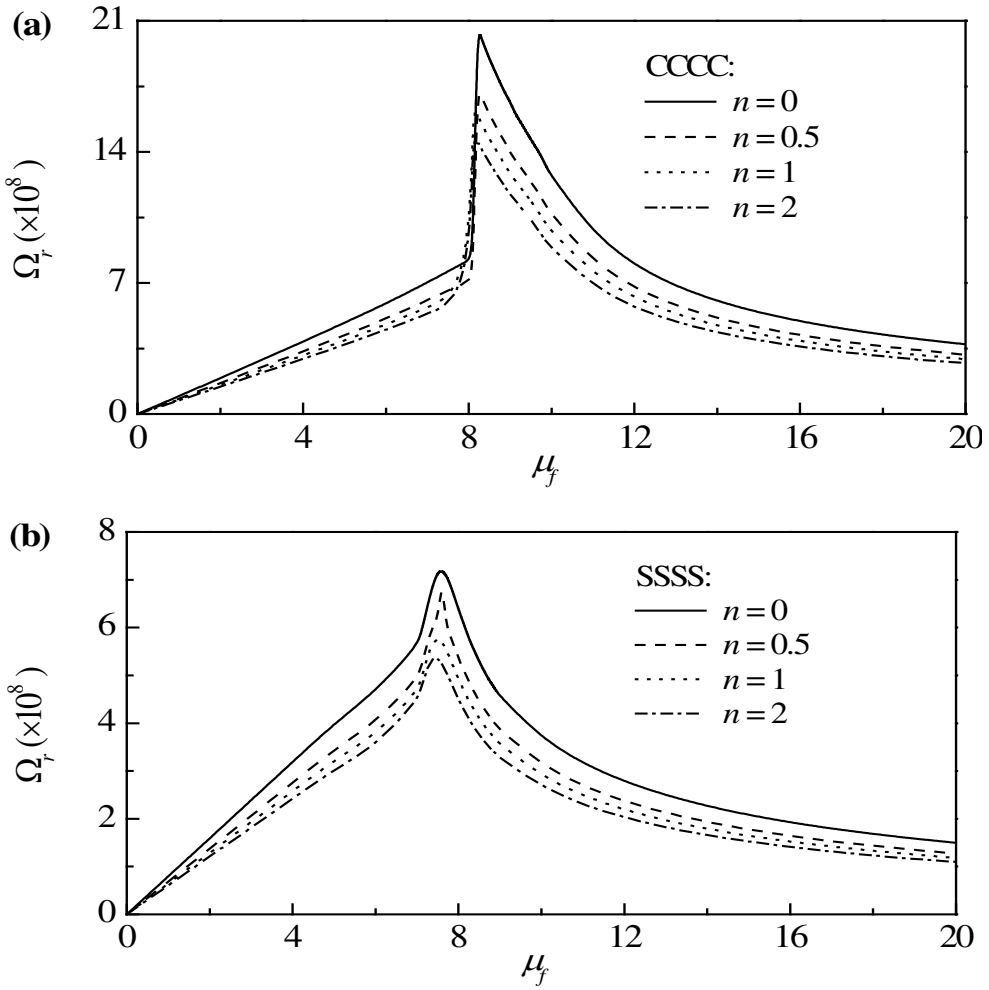

Figure 9. The effect of the gradient index n on the damping characteristic coefficient ~ viscosity curves of CCCC and SSSS FGM microplates (L_x / L_y = 10, L_x / h_0 = 10, h_0/ l = 1, h_f / h_0= 10, ρ_f = 1000 kg/m^3): (a) CCCC and (b) SSSS.

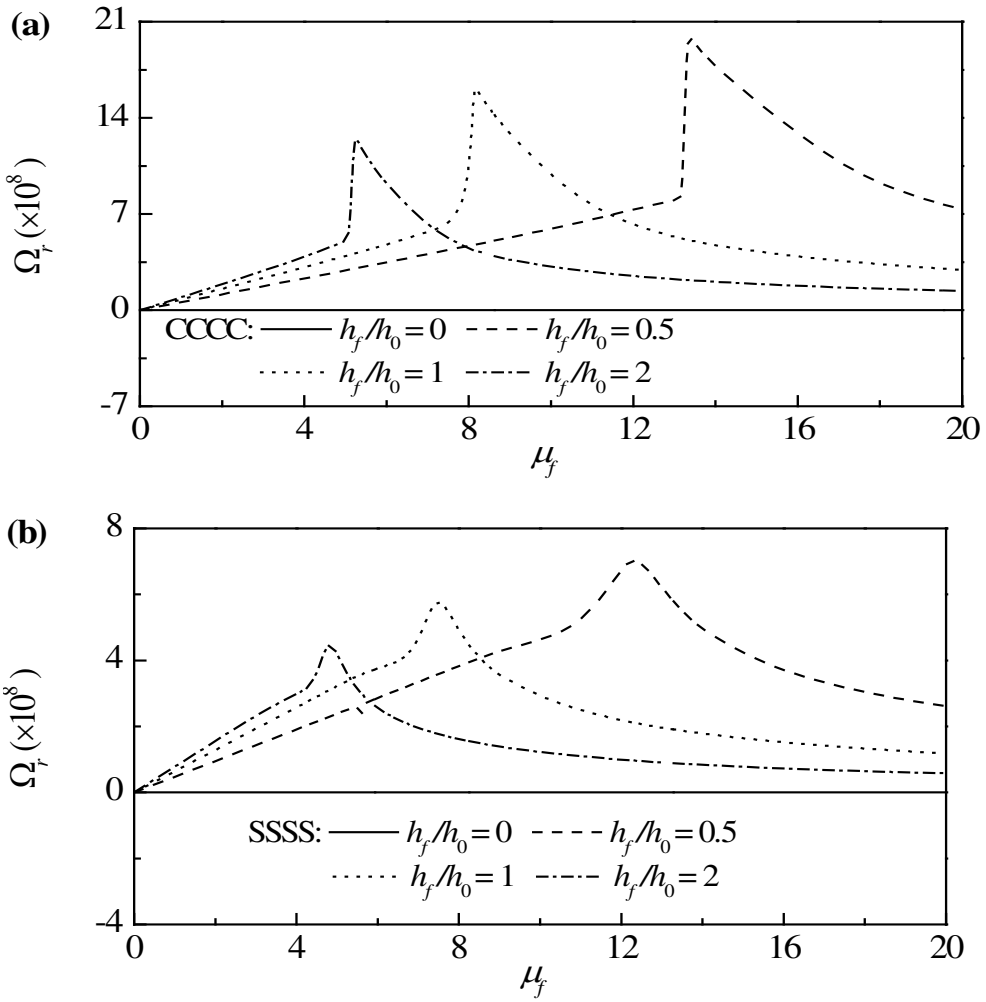

Figure 10. The effect of the fluid height h_f / h_0 on the damping characteristic coefficient ~ viscosity curves of CCCC and SSSS FGM microplates (L_x / L_y = 10, L_x / h_0 = 10, n = 1, h_0/ l = 1, ρ_f = 1000 kg/m^3): (a) CCCC and (b) SSSS.

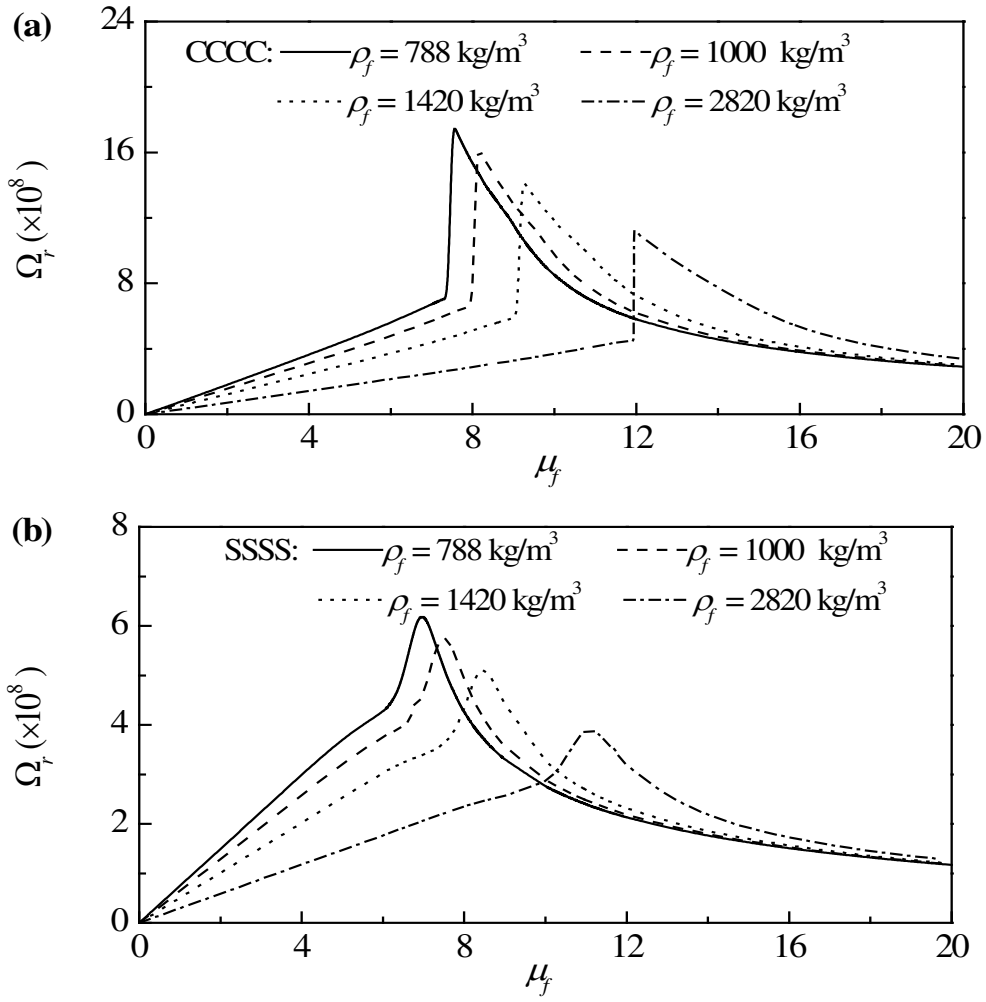

Figure 11. The effect of the fluid density ρ_f on the damping characteristic coefficient ~ viscosity curves of CCCC and SSSS FGM microplates (L_x / L_y = 10, L_x / h_0 = 10, n = 1, h_0/ l = 1, h_f / h_0= 10): (a) CCCC and (b) SSSS.

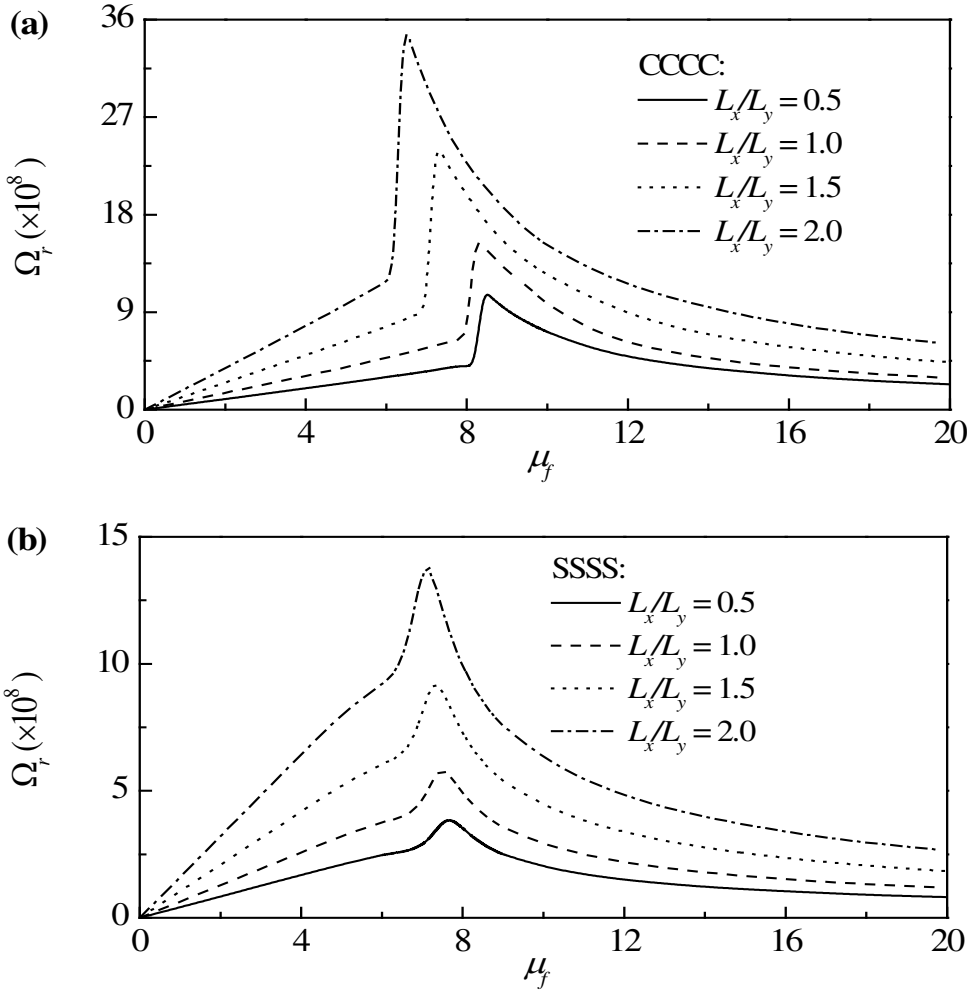

Figure 12. The effect of the aspect ratio L_x / L_y on the damping characteristic coefficient (Ω_r) ~ viscosity (μ_f) curves of CCCC and SSSS FGM microplates (L_x / h_0 = 10, n = 1, h_0/ l = 1, h_f / h_0= 10, ρ_f = 1000 kg/m^3): (a) CCCC and (b) SSSS.

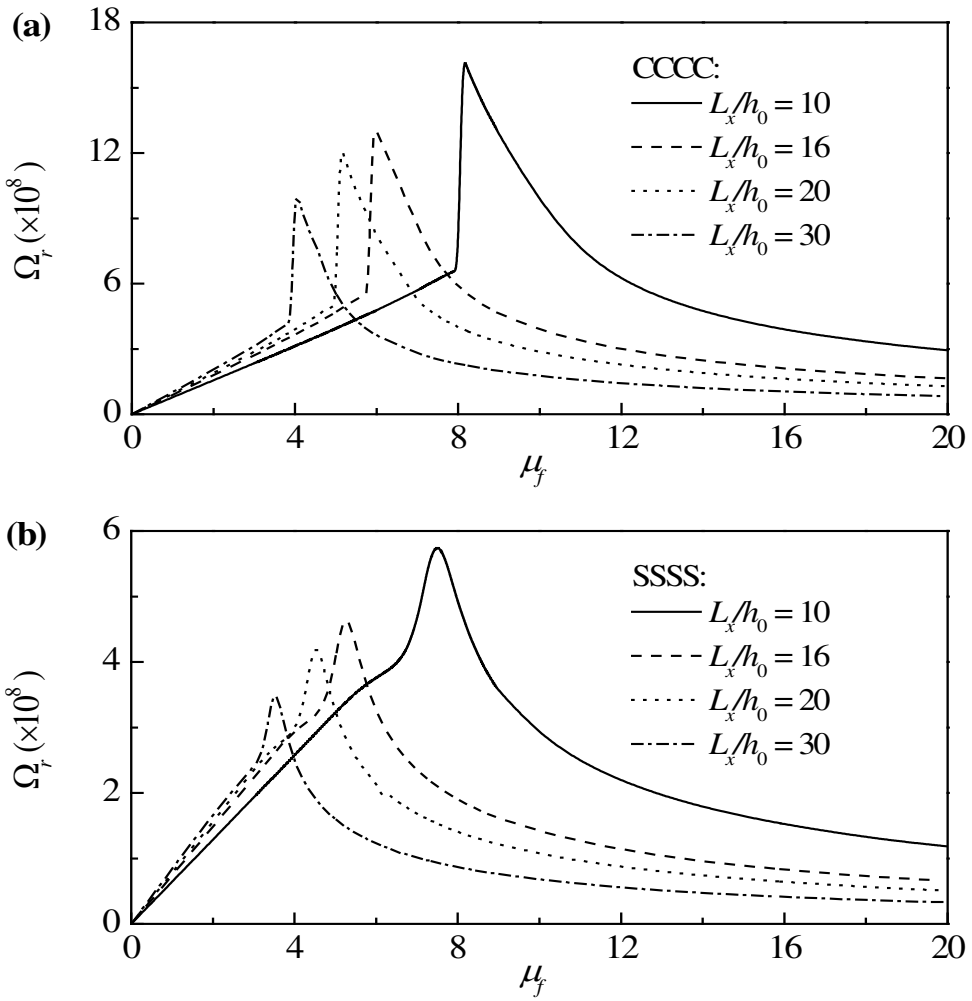

Figure 13. The effect of the slenderness ratio L_x / h_0 on the damping characteristic coefficient ~ viscosity curves of CCCC and SSSS FGM microplates (L_x / L_y = 10, n = 1, h_0/ l = 1, h_f / h_0= 10, ρ_f = 1000 kg/m^3): (a) CCCC and (b) SSSS.